

# Imaging plasticity and structure of cortical maps in cat and mouse visual cortex

Dissertation

At the faculty of Biology

of the

Ludwig Maximilians University Munich

Submitted by

Sven Schuett

from Frankfurt/Main, Germany

21.5.2001

To Christel Stöppler

Tag der mündlichen Prüfung: 3.August 2001

Erstgutachter: PD Dr. Hübener

Zweitgutachter: Prof. Neuweiler

## Acknowledgements

First of all, I would like to thank Dr. Mark Hübener for the wonderful time and the funny moments I could share with him, while he supervised my thesis. Everytime I asked for help, discussion, or advice he was immediately supportive and encouraging. He treated me as if I were a colleague, rather than a student. Thereby, he created an atmosphere, in which discussions could flourish and were most inspiring and humorous. I cannot imagine completing my thesis without him.

I am also very grateful to Dr. Tobias Bonhoeffer, who took interest and time, whenever I asked for it. I particularly valued both his willingness to strongly support all my projects as well as his counsel regarding scientific problems and personal career plans.

Immensely helpful was Iris Kehrer; without her, many experiments would have failed. In particular, I profited much from her profound anatomical skills and from the pleasant time with her. Moreover, I very much appreciated the technical instruction and aid from Volker Staiger, Wilhelm Bulka, and Frank Brinkmann.

In addition, I would like to thank all members in my lab, who greatly facilitated my work by providing a friendly and joyful climate. I will miss the lunch break discussions and the familiarity as well as the very helpful colleagues and friends. Amongst them I would like to thank Albrecht Kossel, Valentin Nägerl, and the former member Frank Sengpiel for comments on parts of the manuscript.

Without my parents' readiness to make possible every decision and step I took, I would not have even started this thesis. I will not be able to repay them for the freedom I was given. Moreover, I thank them for proofreading the manuscript.

Furthermore, my flatmates and friends comforted me in millions of ways during these two years. Without their joy, humor, and care I wouldn't have been able to complete this thesis. Most of all, I am deeply indebted to Steffi, who accepted my decision to start this thesis in Munich. I did not dare to hope that she would accompany me throughout this time. Without her, I wouldn't have wanted to complete this or any other work.

# Content

<b>INTRODUCTION .....</b>	<b>6</b>
<b>PART I PAIRING INDUCED CHANGES OF ORIENTATION IN CAT VISUAL CORTEX.....</b>	<b>8</b>
<b>I.1 METHODS .....</b>	<b>9</b>
I.1.1 IMAGING .....	9
I.1.2 PAIRING PROCEDURE .....	10
I.1.3 ANALYSIS OF FUNCTIONAL MAPS .....	11
I.1.4 ELECTROPHYSIOLOGY .....	12
<b>I.2 RESULTS.....</b>	<b>12</b>
I.2.1 PAIRING-INDUCED SHIFT IN ORIENTATION PREFERENCE .....	13
I.2.2 ANTI-PAIRING CAUSES SHIFT AWAY FROM ANTI-PAIRED ORIENTATION .....	18
I.2.3 SPATIAL DISTRIBUTION OF PAIRING EFFECTS .....	20
I.2.4 STABILITY OF GENERAL STRUCTURE OF THE ORIENTATION MAP .....	24
<b>I.3 DISCUSSION .....</b>	<b>25</b>
I.3.1 PAIRING AND ANTI-PAIRING .....	26
I.3.2 DISTRIBUTION OF PLASTICITY .....	27
I.3.3 STABILITY OF ORIENTATION PREFERENCE MAPS .....	30
<b>PART II MAPPING RETINOTOPIC STRUCTURE AND INHIBITION IN MOUSE VISUAL CORTEX WITH OPTICAL IMAGING.....</b>	<b>31</b>
<b>II.1 METHODS.....</b>	<b>31</b>
II.1.1 SURGERY .....	32
II.1.2 IMAGING AND VISUAL STIMULATION .....	32
II.1.3 ELECTROPHYSIOLOGY.....	33
II.1.4 ANALYSIS .....	33
II.1.5 ANATOMY .....	35
<b>II.2 RESULTS.....</b>	<b>36</b>

II.2.1 RETINOTOPIC ORGANIZATION OF AREA 17.....	36
II.2.2 CORTICAL MAGNIFICATION FACTOR .....	41
II.2.3 LATERAL INHIBITION .....	43
II.2.4 EXTRASTRIATE CORTICAL AREAS .....	48
<b>II.3 DISCUSSION.....</b>	<b>49</b>
II.3.1 AVERAGING THE INTRINSIC SIGNAL ACROSS ANIMALS.....	50
II.3.2 INTER-OCULAR ALIGNMENT OF RETINOTOPIC MAPS .....	50
II.3.3 CORTICAL MAGNIFICATION FACTOR AND GANGLION CELL DENSITY .....	51
II.3.4 OPTICAL IMAGING OF INHIBITION .....	51
II.3.5 EXTRASTRIATE AREAS .....	52
II.3.6 IMAGING MOUSE RETINOTOPY AS A TOOL FOR THE STUDY OF TRANSGENIC ANIMALS....	54
<b>PART III EXTRACTION OF BLOOD VESSEL RELATED ARTIFACTS FROM OPTICAL IMAGING DATA .....</b>	<b>55</b>
<b>III.1 METHODS .....</b>	<b>56</b>
III.1.1 SURGERY AND OPTICAL IMAGING .....	56
III.1.2 BLOOD VESSEL EXTRACTOR .....	57
<b>III.2 RESULTS .....</b>	<b>62</b>
IMPROVEMENTS OF THE BVE .....	66
<b>III.3 DISCUSSION .....</b>	<b>67</b>
<b>SUMMARY.....</b>	<b>69</b>
<b>REFERENCES .....</b>	<b>71</b>

## Introduction

Visual cortical areas of higher mammals contain ordered maps for a number of stimulus properties such as receptive field position and orientation of bars, and for ocular dominance (Talbot and Marshal, 1941; Hubel and Wiesel, 1963; Blasdel and Salama, 1986; Ts'O et al., 1990; Hübener et al., 1997). Although it is well established that the formation of many of these maps depends on sensory input during a phase in development (“critical period”, Wiesel and Hubel, (1963); Blakemore and Cooper, (1970); Hirsch and Spinelli, (1970); Sengpiel et al., (1999)), it is largely unknown to what extent genetic or intrinsic factors control cortical map formation. Furthermore, the exact mechanism of activity dependent plasticity in cortical maps as well as its dependence on specific functional domains have not been identified, yet.

The first set of experiments (part I of this thesis) was aimed at studying the role of activity dependent plasticity for cortical map development. In general, it is assumed that correlated activity in the synaptically coupled neurons leads to enhancement of the activated synapses (Hebb, 1949; Bliss and Gardner-Medwin, 1971; Gustafsson et al., 1987). However, a number of recent studies based on single cell recordings have revealed a more complex relation between synaptic activity and plasticity. It was shown that a spike-time-dependent switch determines the direction of plasticity (Debanne et al., 1994; Markram et al., 1997; Bi and Poo, 1998; Debanne et al., 1998; Zhang et al., 1998; Feldman, 2000): if the postsynaptic neuron becomes depolarized after the presynaptic neuron is active their synaptic connection is potentiated. Conversely, the synapse is weakened if the postsynaptic cell is depolarized before synaptic activation. A spike-time-dependent learning rule for synaptic transmission in the cortex would have important implications for our understanding of cortical map formation. However, it is unknown whether such a mechanism is operational. To study the impact of millisecond timing on cortical plasticity, a pairing paradigm initially introduced by Fregnac et al. (1988) was modified and used to induce changes in orientation preference maps in cat visual cortex: a brief visual stimulus of one grating orientation was paired with brief intracortical electrical stimulation. By varying the relative time-interval between these two stimuli on a millisecond time scale, we investigated whether the direction of plasticity depends on this relative timing. Using this pairing paradigm in combination with optical imaging of intrinsic signals (Grinvald et al., 1986; Ts'O et al., 1990) it became possible to analyze spike-time-dependent plasticity on the level of cortical maps.

In addition, since optical imaging can resolve the detailed spatial structure of cortical maps across a large brain area, it became feasible to measure the dependence of plasticity upon certain

functional domains. We could thus pinpoint sites of high and low potential to undergo plastic changes. Measuring this dependence could help to unravel molecular factors controlling the distribution of plasticity across functional domains in the cortex.

While many studies demonstrated the potential of cortical maps to undergo activity-dependent modification, evidence has accumulated in recent years that ocular dominance maps in the primary visual cortex (Crowley and Katz, 1999; Crowley and Katz, 2000) and retinotopic projections in the superior colliculus (Baier and Bonhoeffer, 1992; Cheng and Flanagan, 1994; Drescher et al., 1995; Itasaki and Nakamura, 1996; Frisen et al., 1998) are predetermined by genetic factors. In higher mammals like cats, however, studying genetic determinants of cortical map formation is difficult. In contrast, the use of transgenic mice permits screening for such factors. Unfortunately, the functional properties of mouse visual cortex are less well understood than those of higher mammals and an efficient technique to screen mice for genes influencing cortical map formation is still missing. Therefore, as a starting point for such studies, we used optical imaging to visualize the retinotopic map in mouse visual cortex (part II). The retinotopic structure in area 17 could be imaged with high reproducibility allowing for detailed quantitative analysis and activity in several extrastriate areas could be recorded.

Both of the above-described parts of this thesis required high quality optical recordings: in the pairing study, relatively small alterations in the cortical maps had to be detected when comparing recordings taken before and after pairing. In mice, the small size of the activated cortical area and the requirements for digital image analysis necessitated highly reproducible maps free of artifacts. Thus, to improve the quality of the imaged maps, an analysis method was developed, which extracted artifacts in intrinsic imaging data based on their relationship to the superficial blood vessel pattern (part III).

## **Part I      Pairing induced changes of orientation in cat visual cortex**

The visual cortex of higher mammals contains regular maps for a number of essential stimulus properties, including orientation, ocular dominance, direction of movement, and spatial frequency. The orientation preference map is characterized by mostly smooth changes of the preferred orientation across the cortical surface. In addition, this map exhibits singularities where orientation preference changes rapidly, giving rise to a pinwheel-like arrangement of orientation domains in the visual cortex (Bonhoeffer and Grinvald, 1991).

While many experimental as well as theoretical studies have investigated the development of orientation preference maps, it is still unclear to what extent activity dependent mechanisms contribute to the formation of this map: on the one hand, it has been shown that orientation preference maps can develop independently of patterned vision (Gödecke and Bonhoeffer, 1996; Weliky and Katz, 1997; Gödecke et al., 1997; Crair et al., 1998). On the other hand, the proper formation of the orientation preference map requires normal levels and patterns of neuronal activity (Chapman and Stryker, 1993; Ruthazer and Stryker, 1996; Chapman and Gödecke, 2000) and its structure can be modified by altering the visual input, e.g. by stripe rearing (Sengpiel et al., 1999). These changes are thought to occur by a “Hebbian” mechanism, in which synaptic strength increases when pre- and postsynaptic neurons are active simultaneously. Cell-culture experiments (Debanne et al., 1994; Bi and Poo, 1998; Debanne et al., 1998) and slice studies *in vitro* (Markram et al., 1997; Feldman, 2000) as well as single cell recordings *in vivo* (Zhang et al., 1998), however, suggest, that correlated pre- and postsynaptic activity can lead to increases or decreases in synaptic efficacy. It was found that the relative timing between pre- and postsynaptic cells determines the direction of changes in synaptic strength on a millisecond timescale: a synapse becomes potentiated if activity of the pre-synaptic cell is followed by depolarization of the postsynaptic neuron. In contrast, if the action potential of the postsynaptic cell precedes the synaptic input, this synapse is weakened. Such a spike-time dependent rule, if valid also during the development of cortical maps, would have strong effects on how patterns of neuronal activity shape cortical maps. The effects of relative timing have so far only been investigated in single cell studies, either *in vitro* or in the frog tectum (Zhang et al., 1998) so that the consequences for cortical map development are unknown. In rearing experiments (Hirsch and Spinelli, 1970), on the other hand, the relatively imprecise control over the stimulus precludes a rigorous study of the effects of millisecond timing on the development of cortical maps.

To address this question we have adapted and modified an approach first introduced by Fregnac et al. (1988) to induce changes in orientation preference maps: we repeatedly paired a very brief visual stimulus (a grating of one orientation) with electrical stimulation within the visual cortex and investigated the resulting changes in the orientation preference maps by optical imaging of intrinsic signals before and after this pairing procedure. By varying the interval between visual and electrical stimulation, we were able to investigate the effect of the relative timing between activation of thalamo-cortical inputs by the visual stimulus and intracortical electrical stimulation.

We used this well-controlled *in vivo* model of functional plasticity of orientation maps to address the following questions:

(1) Does the relative timing between pre- and postsynaptic activity determine the changes of the orientation preference maps, i.e., can the cortical response to the paired orientation either be enhanced or depressed depending on the relative timing of electrical and visual stimulation? A positive answer to this question would necessitate a reconsideration of theories of cortical map formation (Miller et al., 1999, Shouval et al., 2000), which are currently based on learning rules not dependent on correlations in the millisecond time domain.

(2) It has been suggested that specific locations within cortical maps have a higher capacity to undergo plastic changes than other locations (Crair et al., 1997; Kojic et al., 2000; Trachtenberg et al., 2000). These studies have, however, only addressed ocular dominance plasticity and left open the question whether the plasticity of orientation preference exhibits similar inhomogeneities across the cortical surface.

(3) Stripe rearing studies (Blakemore and Cooper, 1970; Hirsch and Spinelli, 1970; Freeman and Pettigrew, 1973; Sengpiel et al., 1999) have shown that the orientation preference map can be altered by experience. However, due to the fact that no recordings were done before the stripe rearing started, it could not be determined whether these changes affected the general structure of the map or whether pre-existing domains were merely enlarged and reduced in the course of the altered rearing conditions.

## **I.1 Methods**

The experiments were performed in 8-11w old kittens; all procedures were carried out in accordance with local government rules and the guidelines of the Society for Neuroscience.

### **I.1.1 Imaging**

Anesthesia was induced with an i.m. injection of ketamine (20–40 mg per kg) and xylazine (2–4 mg per kg). Animals were tracheotomized and artificially ventilated (60 % N<sub>2</sub>O, 40 % O<sub>2</sub>, 1.5 %

halothane during surgery, 0.7-1.0 % during imaging, and 0.4 % during pairing). ECG, EEG, end-tidal CO<sub>2</sub> and rectal temperature were monitored continuously. After the EEG recording had been started, the animals were relaxed with gallamine triethiodide (Sigma, 10 mg/h/kg) added to an infusion of 5.5 % glucose (80 %), 0.9 % saline (20 %), atropine, and corticosteroid. The skull was opened over areas 17 and 18 and the dura was removed. An oil-filled chamber with a small rubber sealed opening for electrode insertion (Grinvald et al, 1999) or agarose flattened with a cover glass were used to stabilize the cortex for simultaneous imaging and electrical stimulation. The eyes were refracted and focused onto a monitor (Mitsubishi-pro 2020) at a distance of 40 cm with gas-permeable contact lenses. Visual stimuli were produced by a stimulus generator (VSG Series Three, Cambridge Research Systems, Rochester, UK). Stimuli consisted of high-contrast sine-wave gratings of four different orientations (0, 45, 90, or 135°) and two spatial frequencies (0.2-0.3 and 0.6-0.8 cycles/degree), which drifted back and forth at an angular velocity of 1.5 cycles/degree. In some cases, computer-controlled eye-shutters were used for monocular stimulation.

For optical imaging, the cortex was illuminated with light of 707 nm. Images were captured using a cooled slow-scan CCD camera (ORA 2001, Optical Imaging, Germantown, NY), focused about 700 µm below the cortical surface. Between 5 and 10 frames of 600 ms duration were collected during each 3-6 s stimulus presentation, followed by a nine s interstimulus interval during which the next stimulus was presented stationary.

### **I.1.2 Pairing procedure**

Flickering gratings of low spatial frequency (0.2-0.3 c/deg) were combined with electrical stimulation in area 17 or 18. A short visual stimulus (three frames = 21 ms, followed by 123 ms blank time) was used to evoke a temporally constrained neuronal response in the visual cortex. For each visual stimulus, one brief electrical pulse (60 µA, 200 µs duration) at a fixed latency was applied through the tip of a tungsten electrode positioned approximately 300 µm below the cortical surface. The paired electrical and visual stimulation was repeated at 7 Hz for three s. After a blank interval of three s, a grating of the orthogonal orientation was presented in the same fashion but without electrical stimulation. This pairing scheme was continued for 3-4 h. (Fig. 1a,b)

The size and position of the cortical region activated by the electrical stimulus was determined by imaging the response to electrical stimulation alone (Fig. 1c). To ensure that neurons were electrically and visually stimulated during pairing we also imaged the cortical response during this time.

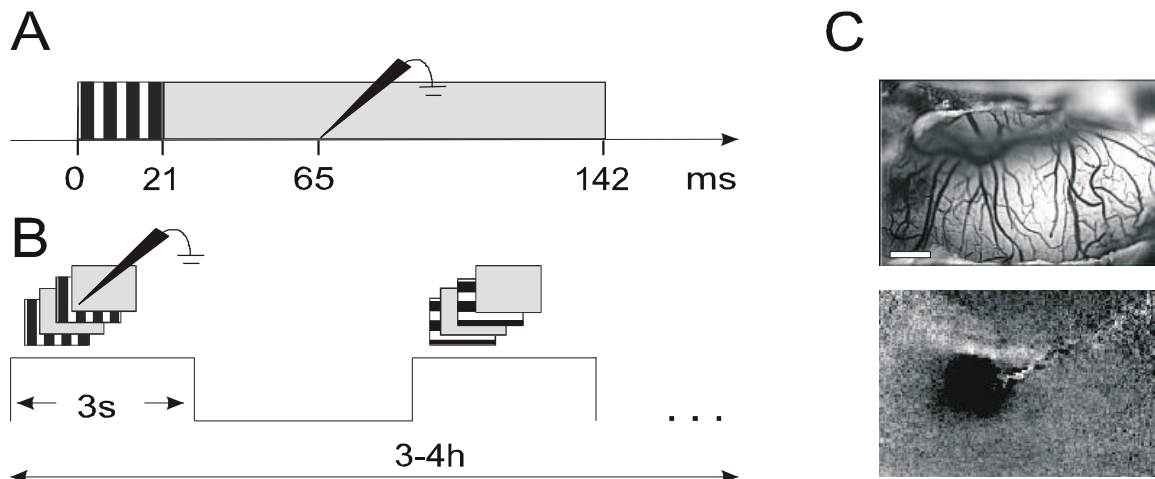


**Figure 1: Schematic of the pairing paradigm. (A)** An orientated grating is very briefly presented on a screen, followed by an electrical stimulus (symbolized by the electrode) delivered to the cortex 65 ms after the onset of the visual stimulus. This sequence is repeated at 7 Hz. The 65 ms delay of the electrical stimulus ensures that neurons in the primary visual cortex are electrically stimulated immediately after visually evoked activity arrives in the cortex. **(B)** Pairing at 7 Hz was continued for 3s, yielding a single pairing trial. Pairing trials were interleaved with similarly flashed presentations of the orthogonal orientation but without concurrent electrical stimulation. The total duration of the pairing was 3-4 hours. **(C)** Optical imaging (32 repetitions) of cortical activity evoked by electrical stimulation alone using the same parameters as for pairing (60 mA, 200 ms, 7 Hz). The tip of the stimulating electrode was located 400  $\mu\text{m}$  below the cortical surface in the center of the dark spot, which corresponds to the activated cortical region. It is partly visible to the left of the activated region. Scale bar within corresponding blood vessel image: 1mm.

To investigate the effect of the relative timing between the electrical and the visual stimulus in the millisecond time-range, we used two latencies for the electrical stimulus: either 65 ms (visually evoked precedes electrically evoked cortical activity; “pairing”) or 35 ms (electrically evoked precedes visually evoked cortical activity; “anti-pairing”) after onset of the visual stimulus.

### I.1.3 Analysis of functional maps

Single-condition responses (averages of 48–96 trials) were divided by the cocktail blank, i.e. by the averaged response to all stimuli. Twelve-bit digitized camera data were range-fitted such that for the iso-orientation maps the 1.5 % most responsive pixels (least responsive pixels) were set to black (white). The signal amplitude was displayed on an 8-bit gray scale. Some images were post-processed with a “blood vessel extractor” algorithm to remove artifacts caused by large blood vessels (Part III of this thesis). For further analysis, all images were low-pass filtered with a Gaussian (45  $\mu\text{m}$ ) and DC shift corrected by subtracting from each image its mean pixel value. Single condition maps presented in the figures were only DC shift corrected, in order to allow for the estimation of pixel noise by eye. Maps obtained before and after the pairing were aligned using the blood vessel pattern.

The change in neuronal response to a particular visual stimulus was quantified in two ways: to evaluate changes in the overall optical response, we computed the difference between the means of pixel values (reflectance signal) before and after pairing. To account for the variance of the signal amplitude we normalized the reflectance signal by the standard deviation of the signal amplitude over space for each animal. Amplitude of the intrinsic signal was defined as the mean standard deviation over space of the intrinsic signal across all maps. As a second more intuitive measure, we thresholded each single condition map at the mean response and measured the size of the area below the mean. The areal measures were normalized to yield a sum of one over all orientations.

These measures were computed in different regions of interest centered on the peak of the optical response to the electrical stimulation in order to determine the magnitude of the pairing effect at different distances from the stimulating electrode.

In addition, we measured the area of induced changes in different regions of functional maps by using masks obtained from the orientation and spatial frequency maps. The mask for one type of orientation domain was obtained by determining those cortical regions, where the response to this orientation exceeded the response to all other orientations. The masks for low and high spatial frequency preference were computed by thresholding the spatial frequency map at the mean of the map taken during presentation of a blank screen. Pinwheel center regions, i.e., cortical regions with rapid changes of orientation preference, were determined by computing the angular derivative of the orientation preference map and thresholding at its mean. The inverse was used as a mask for the pinwheel surround.

### **I.1.4 Electrophysiology**

In one animal, in addition to optical imaging, we carried out electrode recordings before and after pairing at approximately the same cortical locations. We recorded quantitative orientation and direction-tuning curves of multiple single neurons recorded on one electrode and discriminated by their waveforms (Brainware, Oxford, UK). Smooth tuning curves were fitted to the data points based on Fourier analysis (Wörgötter et al. 1989), and preferred orientation and half width of tuning at half height were determined for these curves.

## **I.2 Results**

To induce localized changes in orientation preference maps in kitten visual cortex, we employed a pairing protocol consisting of combined visual and electrical stimulation over a period of 3-4 h. To this end, electrical stimuli were applied to the visual cortex while the animal was stimulated visually with one of four oriented gratings.

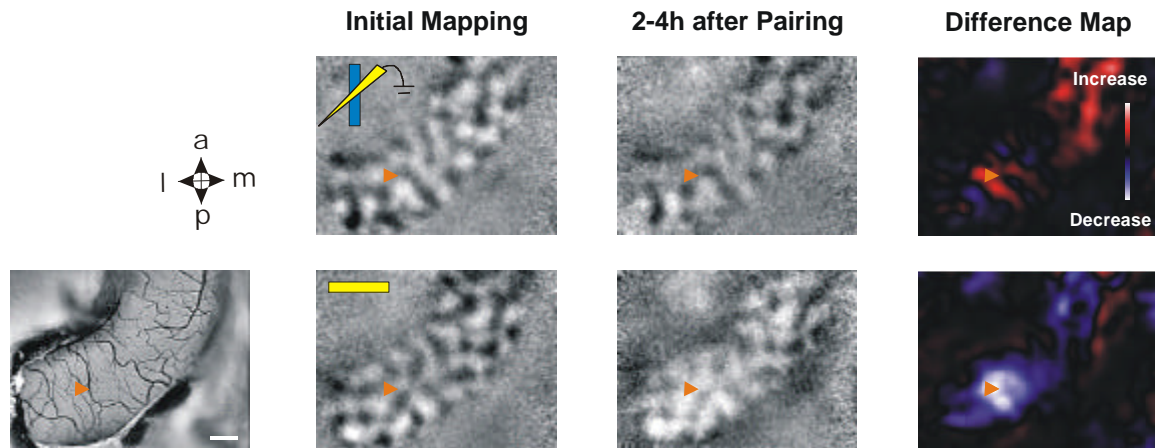


**Figure 2: Optical imaging of pairing induced shifts in orientation preference.** Single condition maps (cocktail-blank corrected) of the paired (top) and orthogonal (bottom) orientation imaged before and after pairing. The arrowhead marks the position of the stimulation electrode. The difference maps show the difference between the single condition map obtained before and after pairing. Red and blue code for an increase and decrease, respectively, of the intrinsic signal after pairing, i.e., the absorption of light due to neuronal activation. In the single condition and the difference maps an increase in response to the paired orientation and a decrease to the orthogonal orientation occurs around the site of stimulation marked by the arrowhead. Left: Blood vessel pattern and orientation of recorded cortical area ((a)nterior, (p)osterior, (m)edial, (l)ateral). Scale bar: 1mm.

To establish a precise timing between visual and electrical stimulation, we used a flickering grating (7 Hz) of one orientation with only 21 ms on time as visual stimulus (Fig. 1a). Based on the known response latencies of neurons in cat area 17 (46.7 ms, Ikeda and Wright, 1975), the interval between the visual and electrical stimulus was chosen such that, for cells in the cortex, activation by the visual stimulus either preceded (pairing) or followed (anti-pairing) the electrical stimulus. As a control, these stimulation trials were interleaved with presentation of the orthogonal orientation (Fig. 1b). The effectiveness of the electrical stimulus in driving cortical cells as well as the size and position of the activated cortical region was determined by optical imaging (Fig. 1c).

### 1.2.1 Pairing-induced shift in orientation preference

In the first set of experiments, we tested whether the response to the paired orientation is enhanced when visual stimulation of neurons in the visual cortex by thalamo-cortical fibers precedes electrical stimulation within the cortex. To measure changes in orientation preference we imaged maps before and 1-6 hours after the pairing, using the same spatial frequency, which was presented during the pairing procedure. In Figure 2 examples of single condition maps of the paired and the orthogonal orientation are presented. The color-coded difference map displays the difference between the single condition maps imaged before and after pairing. In this map red codes for an increase of the intrinsic signal after pairing, while blue codes for a signal decrease. A

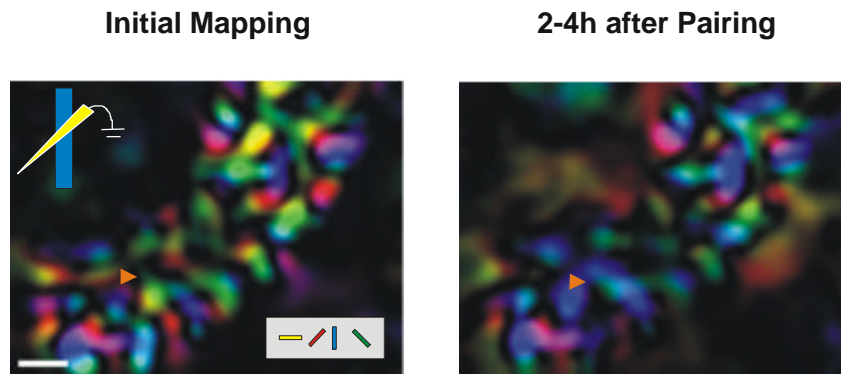


**Figure 3: Polar maps of pairing induced shifts in orientation preference. Color codes for orientation preference and color saturation for orientation selectivity. Note the prominent increase in response to the paired orientation compared to the orthogonal orientation around the site of stimulation after pairing. Scale bar: 1mm.**

comparison of the single condition maps as well as the difference maps show that at the site of stimulation the cortical response to the paired orientation increased substantially after pairing relative to the response of the orthogonal orientation. This orientation specific change becomes even more obvious when comparing the polar maps (Ts'O et al., 1990), which display orientation preference by color and orientation selectivity by saturation (Fig. 3). The polar map taken before pairing shows an equal distribution of all orientations (data not shown). After the pairing procedure, blue patches occur around the site of stimulation, which indicates that the response to the paired orientation is enhanced.

While the shift in orientation preference is visible mainly at the site of stimulation in area 17, a shift can also be detected at some distance within area 18 in the 2 of 6 experiments, in which the optically recorded region comprised the area 17/18 border. The strong activation of area 18 neurons during pairing could account for this effect: the visual stimulus employed during pairing had a low spatial frequency and was presented at a high temporal frequency (7 Hz), thus it is likely to drive neurons in area 18 more strongly than cells in area 17 (Movshon et al., 1978). At the same time it can be expected that the electrical stimulus in area 17 will also activate cells in area 18 via retinotopically organized connections between the two areas (Ferrer et al., 1988).

We quantified the pairing induced changes in cortical area responding preferentially to each of the four orientations at the site of stimulation in six animals (Fig. 4a, paired orientation  $+28\pm 3\%$ , orthogonal orientation  $-24\pm 3\%$  of total area, throughout this paper error is given as standard error of the mean (SEM)). The cortical region activated by the electrical stimulus was determined as shown in Figure 1c and the overall change of the intrinsic signal in this region was computed for each orientation (paired orientation  $72\pm 26\%$  of the mean amplitude of the intrinsic signal, orthogonal orientation  $-70\pm 52\%$ , Fig. 4b).

In every experiment both the cortical area and the overall intrinsic signal corresponding to the paired orientation increased, while both measures decreased for the orthogonal orientation, which was presented during the pairing period but without electrical stimulation. It is evident that the variance of the intrinsic signal change is much larger than that of the areal change. The reason for this difference is most likely that the intrinsic signal differs quite strongly between animals, partly due to different physiological and imaging conditions. Moreover, the area measure is normalized, thus leading to smaller inter-animal variations. The cortical regions activated by the paired orientation increased by nearly a factor of two at the site of stimulation and the difference between the change in area of the paired and orthogonal orientation was highly significant ( $p = 0.0013$ , t-test). The shift in orientation preference did not occur in one control animal where we inserted an electrode and did not stimulate electrically but only visually during an otherwise normal “pairing” protocol.

To illustrate the shift in orientation preference in combination with the magnitude of change, we constructed a “change map” by color-coding the difference in orientation preference with the same color code as the one used for polar maps (Fig. 5a). Thus, instead of using single condition maps for this computation, the orientation vector was calculated for the difference maps shown e.g. in Figure 2. Additionally, in these change maps lightness indicates the size of shift in orientation preference as the relative difference between the paired and unpaired orientation: for example, a strong shift towards the paired vertical orientation results in a light blue patch while a yellow patch indicates a shift towards the horizontal orientation. In addition to illustrating the effect of the pairing the change map also reveals its distribution across the cortical surface: as substantiated by quantification in concentric rings of increasing diameter around the site of stimulation, the magnitude of change in orientation preference decays with radial distance from the site of stimulation (Fig. 5b).

In this quantification, we excluded regions in area 18 which were more than 5 mm distant from the stimulation site.

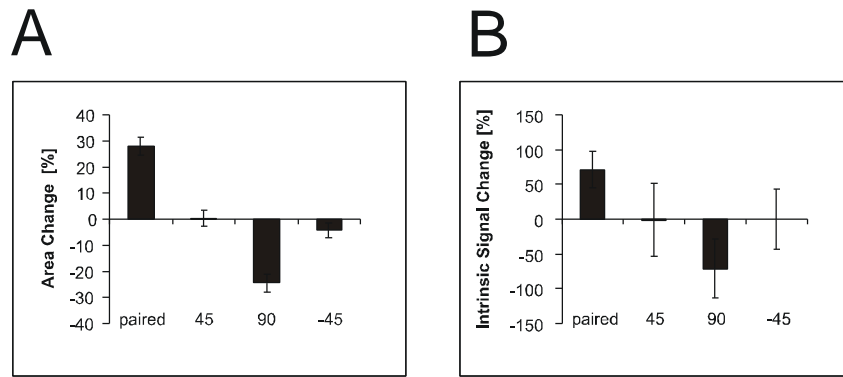


**Figure 4: Quantification of the pairing effect in 6 animals. (A) We measured the pairing induced change in cortical area responding preferentially to each orientation at the site of stimulation. Error bars are SEM. Additionally, the corresponding change in the integral of the intrinsic signal was computed for each orientation (B).**

To further validate the pairing induced shift in orientation preference, we recorded from single units in one animal before (72 cells) and after (76 cells) pairing. To sample from approximately the same cortical sites before and after pairing, we used the cortical blood vessel pattern to position the recording electrode. Comparing all cells recorded before and after pairing a mean shift of  $19.3 \pm 2.9^\circ$  towards the paired orientation occurred, which was highly significant ( $p = 0.00002$ , Wilcoxon Rank test). In 4 out of 6 penetration sites, this shift was found to be significant ( $p < 0.03$  Wilcoxon Rank test, Fig. 6a). To cross-validate optical and electrical recordings, we correlated the orientation preference as determined from optical and electrical recordings at the recording sites. As expected, both, before and after the pairing, the values proved to be well correlated (correlation coefficient: 0.96, Fig. 6c).

Remarkably, only at those five positions where a change towards the paired orientation was detected with the single cell recordings, optical imaging revealed a shift towards the paired orientation. Interestingly, orientation selectivity, measured as the half width at half height of the Fourier-filtered tuning curve, did not change significantly. Likewise, the overall shape of the tuning curves did not exhibit significant differences when we compared the averaged tuning curves aligned by their preferred direction for each orientation.

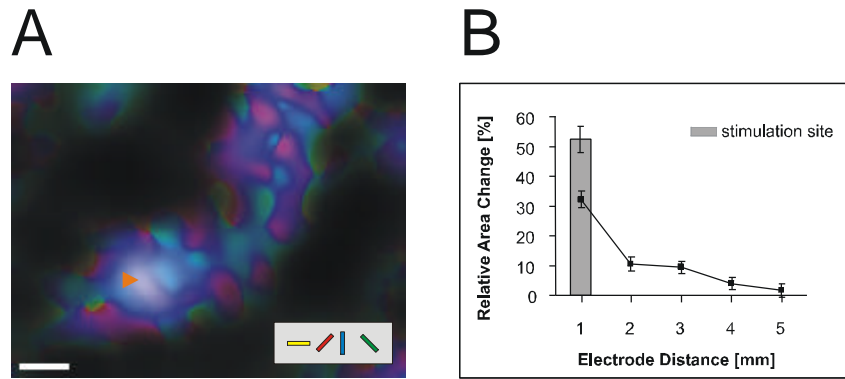


**Figure 5: (A) The change map displays the shift in orientation preference using the same color code as the one used for the polar maps in Figure 3 but employing the difference maps rather than the single condition maps. Lightness indicates the strength of shift towards the paired orientation. (B) Decay of the pairing-effect with increasing distances from the site of stimulation. The relative change in size between paired and orthogonal orientation was quantified in concentric rings around the stimulation site (n = 6).**

This latter result implies that, for instance, no secondary peaks in orientation preference were induced by the pairing procedure. Also, spontaneous rate and direction preference remained unchanged (all p values > 0.1, t-test). Thence the observed changes in the orientation preference maps are most likely caused by a real shift in orientation preference and not by a widening of the orientation tuning curves (Sengpiel et al., 1999). Notably, we recorded neurons 5 to 14 hours after the pairing, implying that the changes remain for this period, at least. We confirmed this also by imaging orientation preferences 14-18 h after pairing in one cat, in which the shift was still present.

Taken together these results show that the pairing paradigm is capable of inducing long-lasting shifts in orientation preference towards the paired orientation. The single unit data corroborate this finding and demonstrate that the effect observed with optical imaging is neither a subthreshold change in orientation preference nor a mere metabolic change.

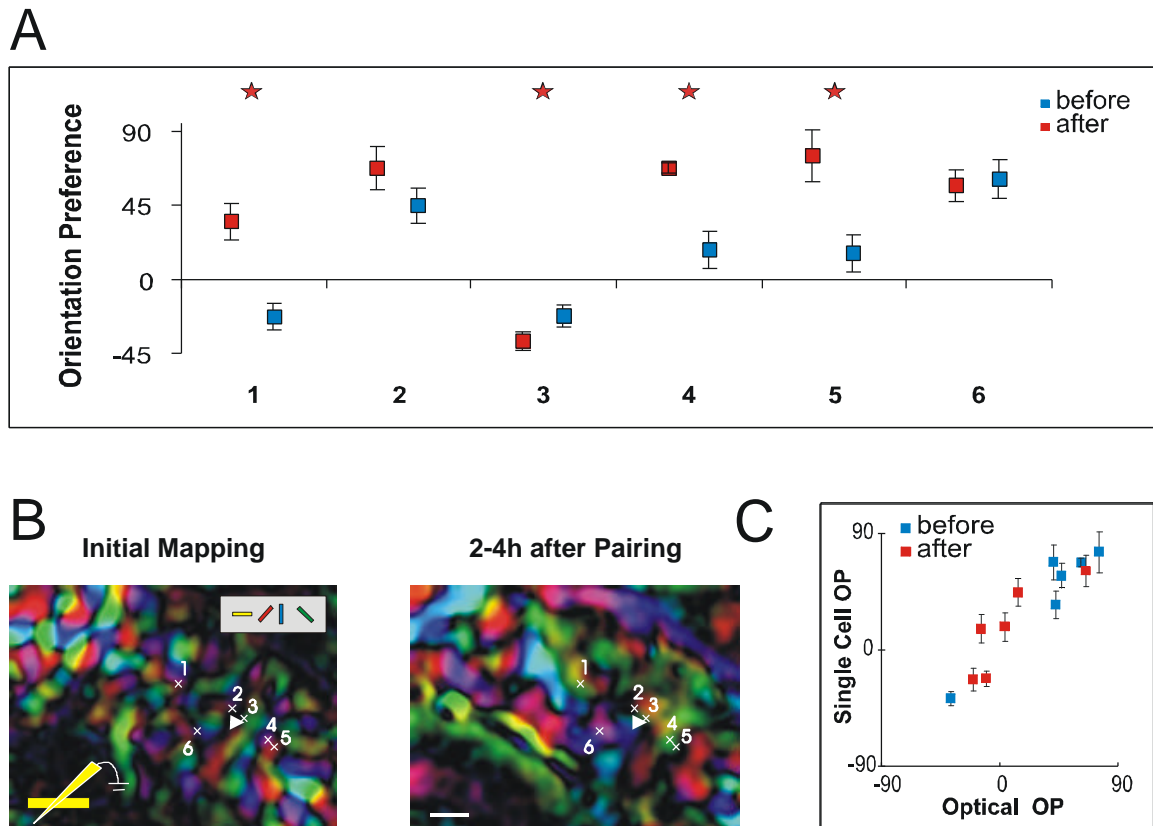


**Figure 6:** Single cell recordings before and after pairing with a horizontal grating. (A) Average orientation preference before and after pairing for each track. The recording positions are marked in the polar maps in (B). Asterisks denote a significant difference before and after pairing ( $p < 0.05$ ); error bars are SEM. (B) Polar maps obtained before and after pairing. The recording sites are marked with numbers, scale bar: 1mm. (C) Scatter plot of optically and electrically measured preferred orientation for each track position before and after pairing. Note that orientation preference recorded after pairing clusters closely around the paired orientation.

## 1.2.2 Anti-pairing causes shift away from anti-paired orientation

In the experiments described above the delay between electrical and visual stimulation was chosen to mimic the pairing paradigm used in single cell studies (Debanne et al., 1994; Markram et al., 1997; Bi and Poo, 1998; Debanne et al., 1998; Zhang et al., 1998; Feldman, 2000), in which presynaptic activation followed by postsynaptic depolarization leads to increases in synaptic strength. To investigate whether the relative timing determines the direction of plasticity for orientation maps in the visual cortex, too, we decreased the temporal delay between visual and electrical stimulation to 35 ms (Fig. 7a). In this anti-pairing paradigm, cells in the cortex are electrically stimulated before the first visually driven activity arrives in the cortex (Ikeda and Wright, 1975).

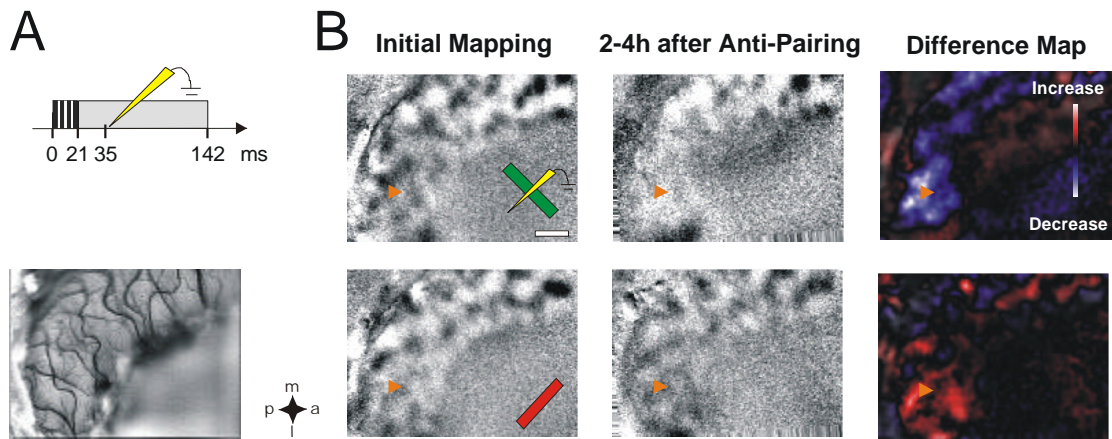


**Figure 7: Optical imaging of the effect of anti-pairing. (A) Schematic illustration of the anti-pairing paradigm: due to the latency of visual responses, the cortex is activated first electrically and then visually. (B) Comparison of single condition maps and difference maps; scale bar: 1mm. In these maps the response to the anti-paired orientation (upper row) decreased after anti-pairing near the stimulating electrode (arrowhead).**

In striking contrast to the effects reported above, the single condition maps of the anti-paired orientations are reduced in strength after the anti-pairing, while cortical neurons respond more strongly to the orthogonal orientation, which was presented during anti-pairing, without a concurrent electrical stimulus (Fig. 7b).

Again, this shift is more obvious when comparing the color-coded polar maps (Fig. 8): orientation domains activated by the anti-paired orientation decrease both in area and intrinsic signal strength, while there is a corresponding increase for the other orientations at the site of stimulation. Quantification of this effect in 4 animals reveals a significant decrease of both the cortical area activated by the anti-paired orientation (anti-paired orientation  $-8.6 \pm 1.2$  %, orthogonal orientation  $+10.6 \pm 2.4$  % of total area,  $p = 0.009$ , t-test, Fig. 9a) as well as its intrinsic signal strength (paired orientation  $-43 \pm 40$  %, orthogonal orientation  $25 \pm 39$  % of the amplitude of the intrinsic signal,  $p = 0.03$ , t-test, Fig. 9b). As is the case for pairing, the degree of change in orientation preference decays with radial distance from the site of stimulation as illustrated by the change map (Fig. 10a,b).

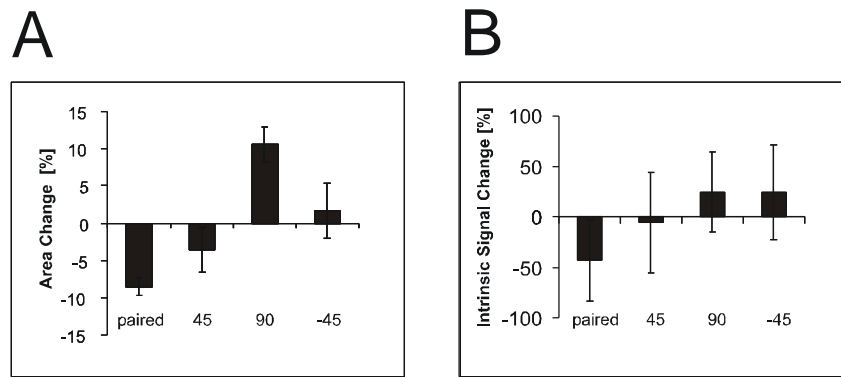


**Figure 9: Quantification (n = 4) of the change in cortical area (A) and intrinsic signal at the stimulation site (B): in contrast to the pairing paradigm, the neural response to the anti-paired orientation decreases.**

Thus, analogous to the effects observed in single cell studies *in vitro*, anti-pairing can reduce neuronal responses to a visual stimulus at the level of cortical maps *in vivo*.

### I.2.3 Spatial distribution of pairing effects

In addition to investigating the effects of the relative timing of pre- and postsynaptic activity on changes in response properties, the spatial resolution of optical imaging made it possible to study the distribution of plasticity in different regions of cortical maps. As a measure for the magnitude of the orientation shift, we employed the relative change in the intrinsic signal between the paired and the orthogonal orientation at the site of the stimulation.

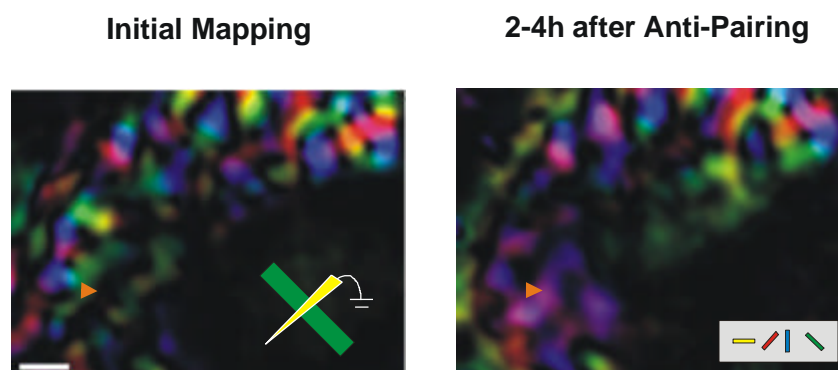


**Figure 8: Polar maps obtained before and after anti-pairing; scale bar: 1mm. After anti-pairing green regions indicating responsiveness to the anti-paired orientation are virtually absent near the stimulating electrode (arrowhead).**

We did not use changes in domain area to quantify the distribution of plasticity across the cortical surface because areal changes are *per se* not equally distributed across the cortex, but are rather confined to the borders of orientation domains. Surprisingly, we did not observe any significant differences between the different orientation domains, i.e., the magnitude of the change was not significantly different within domains for the paired, orthogonal, or intermediate orientations (pairing:  $p = 0.17$ , anti-pairing:  $p = 0.27$ , ANOVA, Fig. 11).

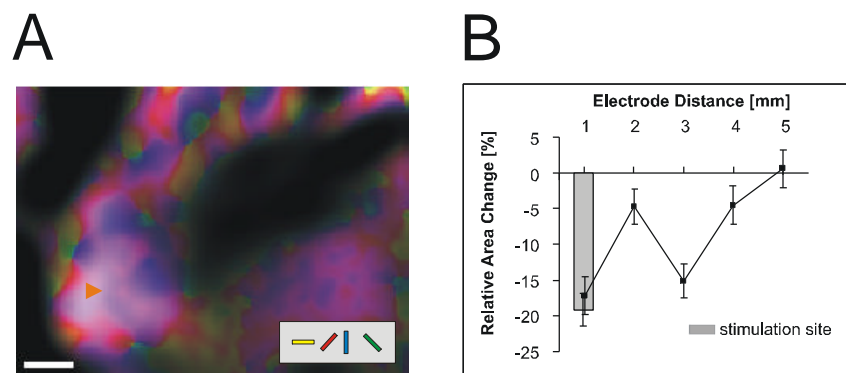


**Figure 10: Illustration of the radial decay with distance from the electrode of the anti-pairing effect by the change map (A) and the quantification using concentric rings around the stimulation site (B).**

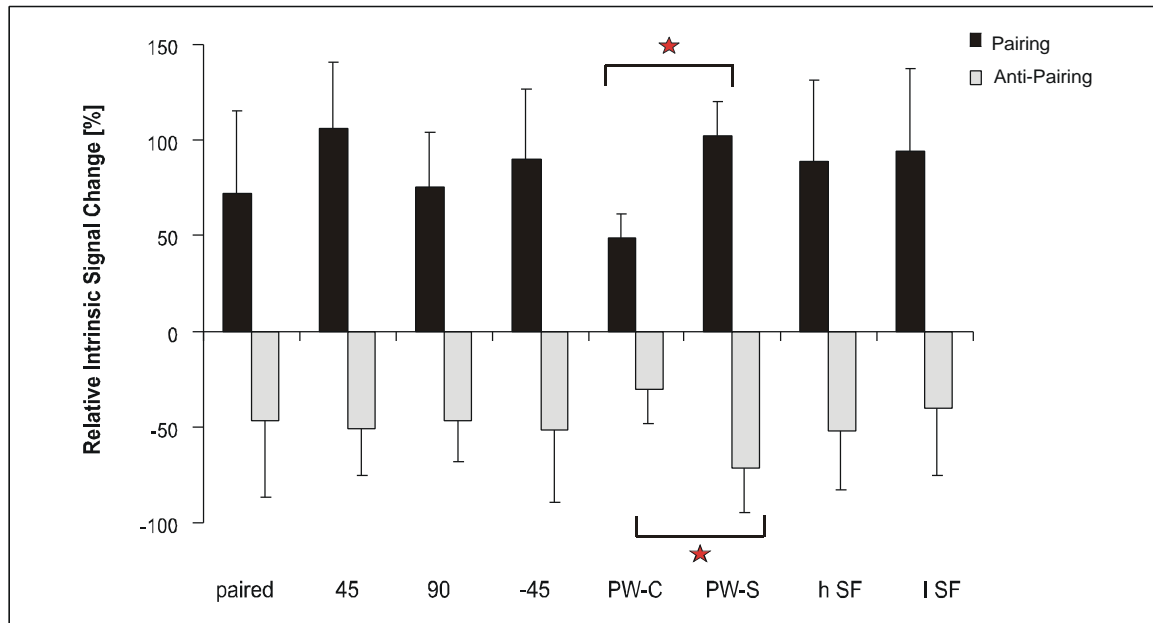


**Figure 11: Spatial distribution of pairing effects across the cortical surface. Relative intrinsic signal change (between paired and orthogonal orientation) in different regions of functional maps after pairing (black) and anti-pairing (gray). While there were no significant differences between domains for the paired, control, or inter-mediate orientations, cortical regions near pinwheel centers (PW-C) showed significantly less change compared to the pinwheel surround (PW-S). No difference was observed between high (h SF) and low spatial frequency (l SF) domains. Asterisks denote significant differences between regions ( $p < 0.05$ ).**

At first glance, this result cannot be explained easily because neurons, which are already tuned to the paired orientation, should not be capable of shifting their orientation any further towards this orientation. We shall return to the possible mechanism underlying this result in the discussion. As for the different orientation domains, there was also no significant difference in the degree of change between low and high spatial frequency domains (pairing:  $p = 0.09$ , anti-pairing:  $p = 0.18$ , t-test). We did, however, find a systematic variation in the size of the shift in different regions of the orientation map: near pinwheel centers the magnitude of plasticity was significantly lower than in regions of the cortex further away from the pinwheel centers (pairing:  $p = 0.02$ , anti-pairing:  $p = 0.03$ , t-test, Fig. 11).

To test whether the inhomogeneous local neighborhood of orientation preferences at pinwheel centers causes their resistance to shifts in orientation preferences, we measured the dependence of the orientation shift magnitude on the local homogeneity of orientation preference. This homogeneity was formalized as the “orientation similarity index”: it quantifies the similarity of orientation preference in the neighborhood of a given point within the cortex. Orientation similarity is high in the pinwheel surround and drops near pinwheel centers. Formally, we determined the orientation similarity index by computing the inverse spatial standard deviation of the orientation maps in a circle with a radius of  $300\mu\text{m}$  around each pixel. We found that the

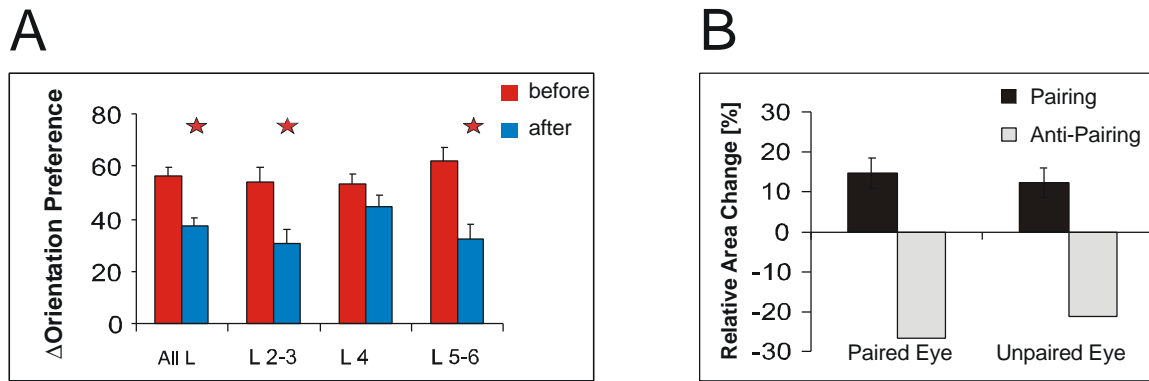


**Figure 12: (A) Layer specific distribution of plasticity as assessed with electrical recordings. The histogram displays the average difference between the cells' preferred orientations and the orientation used for pairing before (red bars) and after (blue bars) pairing for all tracks. Layer 2/3 (L 2/3) and layers 5/6 (L 5/6) exhibited a significant shift ( $p < 0.05$ ) towards the paired orientation, while no significant shift occurred in layer 4 (L 4). (B) Interocular transfer of pairing ( $n = 3$  animals) and anti-pairing ( $n = 1$  animal) induced changes. The (anti-)pairing effect was quantified by measuring the relative change in size between paired and orthogonal orientation for the paired and unpaired eye. The changes in the unpaired eye are almost as strong as in the paired eye.**

correlation between shift magnitude and orientation similarity index is not significantly different from zero when computed in the pinwheel surround (correlation index, pairing:  $-0.21 \pm 0.40$ ,  $p = 0.14$ , anti-pairing:  $0.02 \pm 0.46$ ,  $p = 0.26$ , t-test). This lack of correlation indicates that local neighborhood of orientation preference is not important for induction of plasticity in the orientation domain.

While optical imaging is well suited to study variations in the degree of plasticity across the cortical surface, single unit recordings are necessary to determine the layer specific distribution of plasticity. We therefore used the readings on the micro-drive advancing the electrode to assign cells recorded at different depths in the cortex to different groups, roughly corresponding to different cortical layers. We found that the most significant shift ( $30.8 \pm 6.0^\circ$ ,  $p = 0.001$ , Wilcoxon-Rank test, Fig. 12a) towards the paired orientation occurred in lower layers (presumably layers 5 and 6). It was less pronounced but still significant ( $23.8 \pm 5.7^\circ$ ,  $p = 0.004$ , Wilcoxon-Rank test) in upper layers (layers 2 and 3), while no significant shift in orientation preference was found in layer 4 ( $8.34 \pm 4.2^\circ$ ,  $p = 0.22$ , Wilcoxon-Rank test).

This layer-specific effect is unlikely to result from electrode-penetrations not being oriented orthogonal to the cortical surface. In this case, one would expect a monotonous distribution of the apparent shifts as a function of recording depth. However, we did find a bimodal distribution, with shifts being high in the upper and the lower layers but small in layer 4.

The most straightforward explanation for this observation is that the shift in orientation preference is not caused by changes of thalamo-cortical but rather of cortico-cortical synapses outside layer 4. To substantiate this interpretation, we studied whether the effect of the pairing is transferred

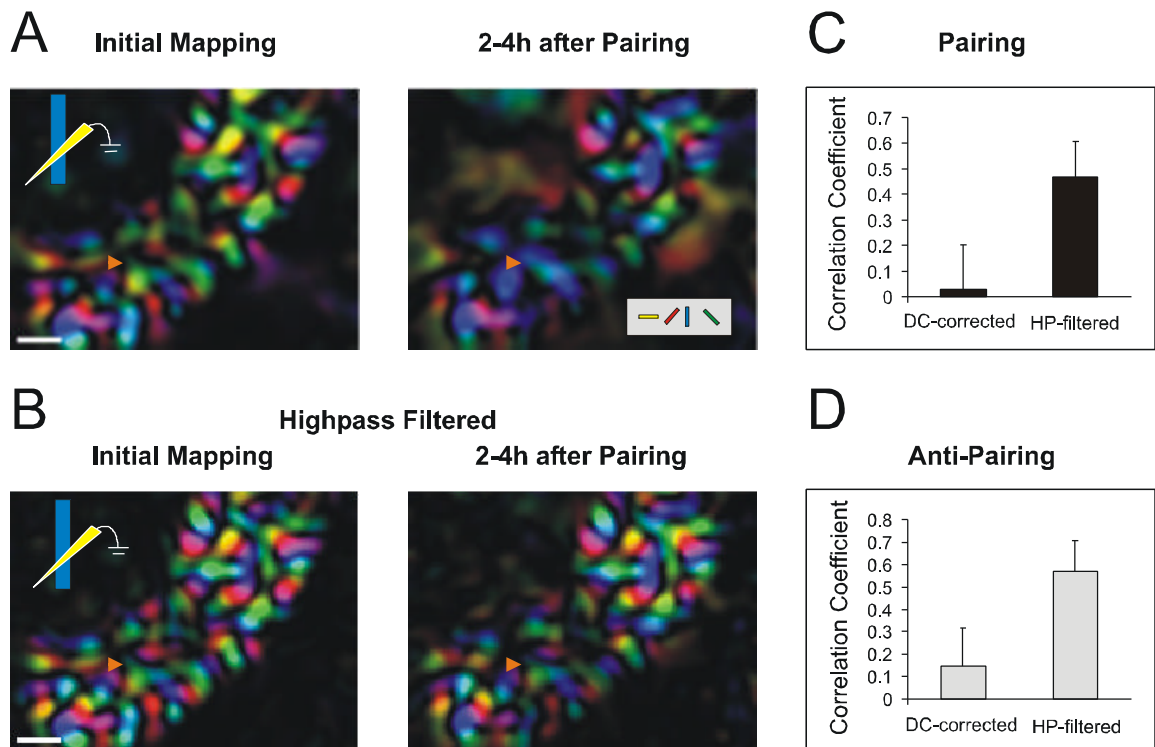


**Figure 13: Stability of the general structure of the orientation map.** Polar maps computed from (A) DC-shift corrected and (B) strongly high-pass filtered (boxcar: 1 mm) single condition maps obtained before and after pairing. The high-pass filtering does not change the overall layout of the maps as indicated by the virtually identical layout of the two polar maps before pairing. Since the plastic effects are on a scale threefold larger than orientation patches, the high-pass filtering extracts the change in orientation preference and leaves the orientation preference map obtained before and after pairing virtually unchanged. Without this filtering a prominent orientation shift is visible. Scale bars: 1mm. The change in general map structure was quantified by correlating the single condition maps with and without high-pass filtering at the site of stimulation for (C) pairing and (D) anti-pairing. The high correlation coefficient calculated after high-pass filtering indicates, that the general map structure is not changed by (anti-)pairing.

from one eye to the other. To this end, we imaged the monocular orientation maps for both eyes, but paired electrical and visual stimulation only for one eye.

If the shift were mainly due to changes of cortico-cortical synapses, a considerable transfer of the effect to the unpaired eye would be expected. Such a transfer did in fact occur, and the degree of shift in the orientation map recorded through the unpaired eye was non-significantly different from the shift of the paired eye ( $p = 0.17$ , t-test, Fig. 12b).

## 1.2.4 Stability of general structure of the orientation map

The results described above clearly show that prominent changes in orientation preference can be induced by a pairing protocol. Does this manipulation also lead to alterations of the general structure of the layout of orientation in the visual cortex? To address this question, we used a simple method to extract global changes in orientation preference from the maps: since the spatial

scale of the changes induced by pairing is roughly threefold larger than the spacing of the orientation domains (Fig. 5a,b and Fig. 10a,b), we applied a strong high-pass filter (1000  $\mu\text{m}$  boxcar) to the single condition maps. This filtering thus extracts the change in orientation preference, while it only marginally affects the general columnar structure, as illustrated by the polar maps computed after high-pass filtering (Fig. 13b).

Comparing otherwise identical polar maps with and without this spatial filtering before pairing reveals that the layout of the maps is virtually insensitive to the high-pass filter (Fig. 13a,b). Importantly, when comparing high-pass filtered polar maps before and after pairing, virtually no change in map layout can be detected, suggesting that the general map structure is left unaltered by the pairing. We quantified the stability of the general map structure by correlating the high-pass filtered single condition maps obtained before and after the pairing near the site of stimulation (Fig. 13c,d). The correlation is not significantly different from control regions further away from the stimulation site ( $p = 0.09$ , t-test). Without high-pass filtering, however, the correlation is significantly reduced ( $p = 0.02$ , t-test). Thus, despite pronounced shifts in orientation preference the observed changes seem to be only superimposed over an otherwise stable structure of the orientation layout.

### **1.3 Discussion**

Plasticity and development of functional maps in the visual cortex have been studied extensively by examining the effects of long-term alterations of the visual input like monocular deprivation (Wiesel and Hubel, 1963; Shatz and Stryker, 1978; Antonini and Stryker, 1993) or stripe rearing (Blakemore and Cooper, 1970; Hirsch and Spinelli, 1970; Freeman and Pettigrew, 1973; Sengpiel et al., 1999) on the cortical architecture.

While a great deal of information on plasticity of cortical maps has been obtained with these studies, rearing experiments have the disadvantage that they do not allow strict control over the stimulus conditions. Relatively precise measurements of determinants of synaptic plasticity *in vivo* with natural stimuli have only been obtained on the single cell level in pairing paradigms using stimulation with potassium or pharmacological agents (Fregnac et al., 1988; Fregnac and Shulz, 1999; Shulz et al., 2000). However, with these paradigms it is not possible to assess detailed temporal aspects of the stimulation like the impact of the relative timing of pre- and postsynaptic activation on the direction of synaptic changes (Debanne et al., 1994; Markram et al., 1997; Bi and Poo, 1998; Debanne et al., 1998; Zhang et al., 1998; Feldman, 2000). In the present study, we have employed a paradigm, which made it feasible to induce plasticity on the level of cortical maps under well-controlled stimulation and recording conditions: we used short visual and electrical stimuli in combination with optical imaging of intrinsic signals.

This pairing paradigm is capable of inducing long-lasting shifts in orientation preference in cat visual cortex. While single cell *in vivo* studies are essentially restricted to the measurement of plastic changes in the range of an hour (Fregnac et al., 1988; Fregnac et al., 1992), we were able to observe pairing-induced effects on the basis of cortical maps for periods up to 24 h. Furthermore, in contrast to rearing experiments, we were able to record the orientation preference maps before and after the pairing both electrically and optically. Thence, a more accurate control and interpretation of experimentally induced neuronal response changes become feasible. Additionally, we found that on a millisecond time-scale the relative timing between visual and electrical stimulation controls the direction of plasticity within the orientation preference maps. Moreover, our results show that the magnitude of this form of plasticity is strongly reduced at pinwheel centers in comparison to the pinwheel surround.

### **I.3.1 Pairing and anti-pairing**

We have shown that orientation preference can be shifted strongly by stimulating the visual cortex first with natural input and immediately afterwards electrically. This type of stimulation can lead to long-lasting changes and it is analogous to a pairing paradigm, which combines presynaptic stimulation and subsequent postsynaptic depolarization of a single neuron, as it is used in single cell studies for the induction of synaptic long term potentiation (LTP, Markram et al., 1997; Zhang et al., 1998; Feldman, 2000). In our experiments, the visual stimulus activates cortical neurons via synaptic potentials, while the electrical stimulus elicits action potentials in cortical neurons mainly by direct depolarization at the axon initial segment (Rattay, 1998). In contrast, fibers of passage or dendritic trees contribute only little to the activation of cortical cells by electrical stimulation (Rattay, 1998). Therefore, it becomes possible to control the relative timing of presynaptic stimulation and postsynaptic activation by altering the interval between visual and electrical stimulation: given that the electrical stimulus is applied after visually evoked signals arrive within the cortex, postsynaptic activation caused by electrical stimulation is likely to follow activation of presynaptic inputs by the visual stimulus.

In contrast to single cell studies, not only excitatory, but also inhibitory circuitry will be recruited by the stimulation and can influence the pairing effect. The strong shunting inhibition caused by the visual stimulus (Borg-Graham et al., 1998) and the electrical stimulation (Chung and Ferster, 1998) are likely to sharpen the timing relation between the visual and electrical stimulation for pairing and anti-pairing, respectively.

The hypothesized timing relations, however, will not hold precisely for all neurons, but will only be statistically valid for neurons around the stimulating electrode. Therefore, we employ optical

imaging which samples the neuronal response from many cells; thence it is suited to detect potential population changes with high variability on the single cell level.

Our results indicate that if the visual (presynaptic) stimulus precedes the electrical (postsynaptic) stimulus the response to the visual stimulus is enhanced, while it is reduced if electrical precedes visual stimulation. A straightforward interpretation of these results consistent with single-cell studies (Debanne et al., 1994) is that the (anti-) pairing paradigm alters synaptic strength within excitatory pathways: accordingly, pairing strengthens excitatory synapses, which contribute to the generation of orientation preference, while anti-pairing depresses those synapses. Cortical orientation selectivity, however, is most likely generated by an interplay of excitatory *and* inhibitory networks (Sillito, 1975; Eysel et al., 1998; Shevelev et al., 1998). Therefore, changes in the inhibitory network could also contribute to the observed shift in orientation preference. It has been shown in slice recordings that GABAergic synapses can also undergo LTP (Komatsu and Iwakiri, 1993) and LTD (McLean et al., 1996), but spike-time dependent plasticity has not been investigated at inhibitory synapses. It is therefore difficult to determine to what extent synaptic changes in inhibitory pathways contribute to the pairing induced effects seen in our experiments. Our data suggest that spike-time dependent plasticity can influence activity-dependent refinement of cortical maps. Modeling studies (Song et al., 2000) have shown that spike-time dependent learning enhances short latency inputs and depresses longer latency input. In the case of orientation preference, this could lead to a sharpening of the orientation tuning because non-optimal synaptic input to a weakly orientation selective neuron will become reduced over time.

### **I.3.2 Distribution of plasticity**

To unravel the impact of synaptic changes on cortical network activity it is necessary to pinpoint the site of changes within the functional network. On the one hand, this facilitates the interpretation of the current results, on the other hand, it might further our understanding of the development of cortical orientation selectivity.

#### **I.3.2.1 Cortico-cortical but not thalamo-cortical synapses are changed**

My electrophysiological data imply that changes occur predominantly at cortico-cortical but not at thalamo-cortical synapses in layer 4, since layer 4 neurons do not shift their orientation preference, while layer 2-3 cells and, even more pronounced, cells in layers 5 and 6 exhibit strong shifts. The inter-ocular transfer of monocular pairing supports this conclusion: if the observed plasticity were mainly due to thalamo-cortical synapses one would expect much smaller transfer to the unpaired eye.

These results are in line with studies on the layer specific distributions of the effects of brief monocular deprivation, in which it was shown that changes are observed first in the upper layers and not in layer 4 (Kossut et al., 1983; Kossut and Singer, 1991; Trachtenberg et al., 2000). The difference found in these studies between granular and extragranular layers with respect to the shift in ocular dominance could in principle be an effect of the difference in the proportion of binocular cells in these layers: a number of studies indicate that binocular cells are more prone to undergo shifts in ocular dominance than monocular cells. It has been shown for example that the ocular dominance columns of the deprived eye shrink mainly in binocular zones (Crair et al., 1997). Moreover, it has been reported that strabismic cats, which have fewer binocular cells (Maffei and Bisti, 1976), are less sensitive to monocular deprivation (Mustari and Cynader, 1981) and recover less readily from prolonged monocular deprivation (Frank Sengpiel, personal communication). Therefore, it could have been argued that the lower number of binocular cells in layer 4 might cause layer 4 to be more resilient to ocular dominance shifts.

Our findings suggest, however, that the layer specific potential to undergo plasticity is not due to differences in the number of binocular cells between layers. Since orientation selectivity, in contrast to ocular dominance, is more or less similar across cortical layers in the cat (Berman et al., 1982), a similar argument cannot explain the resistance of layer 4 cells to pairing induced shifts in orientation preference. Therefore, the lack of plasticity in layer 4 neurons is more likely to be due to layer specific critical periods (Daw et al., 1992; Kirkwood et al., 1995; Kirkwood et al., 1997; Sermasi et al., 1999).

### **I.3.2.2 Equal expression of orientation shift across all orientation domains**

We did not detect any significant differences in the degree of shifts between different orientation domains. This was surprising because *prima facie* one would expect that the shift in domains of the paired orientation should be smaller, since neurons in these domains are already tuned to the paired orientation and thus cannot shift their orientation preference any further. A number of reasons might account for this equal distribution: first, since we have used only four different orientations as stimuli, the orientation preferences of neurons within the optically imaged domains of the paired orientation span a range of  $\pm 22.5$  degrees. In addition, even at a given location in the visual cortex orientation preference varies by about 15 degrees (Albus, 1975; Murphy and Sillito, 1986; Hetherington and Swindale, 1999). Moreover, the visual stimulus used in our pairing paradigm most strongly activates domains of the paired orientation. Therefore, cells in these domains might be most sensitive to pairing induced shifts. Finally, a change in orientation preference measured by optical imaging can be caused either by an actual shift in orientation

preference or by a sharpening of the orientation tuning for the paired orientation only. Taken together, these factors could lead to the observed homogeneous distribution of the pairing effect across all orientation domains.

### **I.3.2.3 Shift in orientation preference is reduced at pinwheel centers**

While the degree of plasticity does not vary between different orientation domains, we observed a significant variation between pinwheel center regions and the pinwheel surround: the most pronounced changes in orientation preference occurred within the pinwheel surround, while significantly smaller shifts were detected near pinwheel centers. This provides direct evidence that plasticity is reduced at the site of pinwheels and other regions of rapid changes in the orientation preference map. This variation could be due to variations in the distribution of plasticity related molecules across the visual cortex (Trepel et al., 1998; Kojic et al., 2000). It has been found that NMDA-receptors are concentrated in the transition zone between ocular dominance columns (Trepel et al., 1998). Since the centers of ocular dominance columns statistically co-localize with pinwheel centers (Crair et al., 1997; Hübener et al., 1997), the NMDA receptor density – and thus possibly plasticity – is expected to be reduced at pinwheel centers. A similar stability of pinwheel centers has been inferred from a recent monocular deprivation study (Crair et al., 1997). Crair et al. found that the small cortical regions maintaining their responsiveness to the deprived eye co-localized with pinwheel centers. In addition to an intrinsic specialization like the suggested NMDA-receptor distribution causing the stability of pinwheel centers, Crair et al. speculated that differences in circuitry might contribute to this stability. In fact, very recently it has been found that the lateral spread of horizontal connections is relatively small at pinwheel centers compared to their surround (Zoltán Kisvárdy, personal communication).

Other explanations, e.g. differences in receptive field properties between pinwheel center and pinwheel surround, are less likely because neurons at pinwheel centers are equally selective for orientation as neurons in the pinwheel surround (Maldonado et al., 1997). Additionally, we excluded that the neurons' ability to shift their orientation preferences depends on a neighborhood of similar orientation preference: the strength of plastic changes within the pinwheel surround is not significantly correlated with the similarity index.

Therefore, the most plausible candidate mechanism to explain the differences between pinwheel centers and surround are variations in the expression of plasticity related molecules. However, to validate this hypothesis further, more molecularly oriented studies will be needed.

### **I.3.3 Stability of orientation preference maps**

Stripe rearing studies (Blakemore and Cooper, 1970; Hirsch and Spinelli, 1970; Freeman and Pettigrew, 1973; Sengpiel et al., 1999) have suggested that specific visual environments can cause quantitative alterations of the layout of orientation domains. The most recent of these studies (Sengpiel et al., 1999) explicitly suggests that the general map structure remains unaltered. However, in none of these studies a direct comparison between the maps before and after induction of shifts in orientation preference was carried out. Comparing the orientation maps obtained in this study before and after pairing revealed clear shifts in orientation preference in large regions of the cortex. To distinguish between mere shifts in orientation preference and change in general structure of the layout, we employed a strong high-pass filter to remove any large-scale changes in orientation preference from the maps and thus demonstrated that the general structure of the maps is preserved despite strong shifts in orientation preference.

In the face of the prominent changes in orientation preference one might wonder why the general structure of orientation preference maps is so rigid. Our finding that plasticity is inhomogeneously distributed within the cortex provides two possible mechanisms contributing to the observed stability: first, pinwheel centers are less sensitive to the induction of plasticity. Therefore, while the centers of orientation domains can shift their orientation preference, pinwheel centers limit this shift and thus preserve the overall structure of the map. Second, the layer-specific distribution of plasticity can further help to reduce shifts in orientation preference in our paradigm: thalamo-cortical connections have been shown to play a major role in determining orientation preference (Chapman and Stryker, 1993; Reid and Alonso, 1995; Ferster et al., 1996), and we have provided evidence that these connections are unlikely to undergo a pairing induced change. Therefore, the relative stability of these connections will also limit potential shifts of the orientation preference map and help to maintain its general structure.

## **Part II Mapping retinotopic structure and inhibition in mouse visual cortex with optical imaging**

The visual cortex of the mouse consists of a number of anatomically (Caviness, 1975; Olavarria et al., 1982) and functionally (Dräger, 1975; Wagor et al., 1980) distinct areas. Whereas mouse primary visual cortex seems to lack any obvious parcellation into certain functional domains, such as ocular dominance, orientation preference, etc., which are prominent in the visual cortex of many higher mammals (Blasdel and Salama, 1986; Ts'O et al., 1990; Hübener et al., 1997), it has been shown that it does contain an ordered retinotopic map (Dräger, 1975; Wagor et al., 1980). However, the detailed layout of this map, the distribution of the cortical magnification factor, as well as the inter-animal variability have not been studied systematically and very little is known about the number and organization of extrastriate areas.

Since the high resolution mapping of cortical areas with electrode recordings is very tedious and error-prone we employed optical imaging of intrinsic signals (Grinvald et al., 1986) to determine the retinotopic structure of mouse visual cortex. Stimulation of the animals at different locations in the visual field and conventional intrinsic imaging technique together with a novel “winner-takes-all” analysis allowed us to obtain highly reproducible retinotopic maps with low inter-animal variability, greatly facilitating the quantitative analysis. Since we imaged cortical activity across the entire visual cortex, we were also able to map out multiple extrastriate areas. In addition, we found that optical imaging indicated a very prominent lateral inhibition within the visual cortex, which was confirmed by electrical recordings.

An obvious motivation for establishing the method of optical imaging in mouse visual cortex is the availability of transgenic mouse technology. Mapping the retinotopic structure of mouse visual cortex is particularly interesting because a central question in neurobiology is the development of topographically ordered projections in the brain (Prakash et al., 2000; Vanderhaeghen et al., 2000). The ease of use and the small inter-animal variability of mapping mouse visual cortex retinotopy by optical imaging permit efficient screening for genetic factors that contribute to the establishment of ordered projections and areal specification in the cerebral cortex.

### **II.1 Methods**

The experiments were performed in ten 7-14w old C57BL/6 as well as in mixed background C57BL/6 x SV/129J mice. In pilot studies, we optimized the methods described here using at first

27 rats and then 9 mice. All procedures were carried out in accordance with local government rules and the guidelines of the Society for Neuroscience.

### **II.1.1 Surgery**

Mice were anaesthetized with a combination of urethane und ketamine (initial anesthesia 2–4 mg/kg ketamine i.m., 10 mg/kg urethane i.p., maintained by continuous i.p. infusion: 1 mg/kg ketamine, 1 mg/kg urethane). This combination of anesthetics was found to be crucial for reproducible high quality imaging and long-term stability of physiological conditions. In particular, to reliably image retinotopic maps, the pupils should not be dilated by the anesthetics or other drugs. We were not able to image these maps when using halothane anesthesia alone or when we applied atropine systemically in pilot experiments on rats, presumably because the pupils were dilated. To prevent dehydration, a mixture of 35 % glucose and 65 % saline was infused i.p. At three ml/kg. The animal was initially positioned stereotaxically using mouth and ear bars, with the mouth bar positioned 3 mm below the inter-aural line. The skin above the skull was cut open and a few drops of silicon oil were immediately applied to the bone to maintain its transparency. The skull was then attached to a head holder with a mixture of glass beads and tissue glue (Histoacryl, Braun, Germany), and the mouth and ear bars were removed. For electrical recording experiments, a trepanation of 4 × 4 mm above the visual cortex was performed after optical imaging. During surgery, the eyes were covered with eye protection cream (Isopto-Max, Alcon Thilo, Germany), which was replaced by silicon oil to prevent drying of the cornea during optical imaging.

In most experiments, the animals breathed spontaneously with a flow of pure oxygen (0.5 l/min) directed to the nose. For experiments with both optical and electrical recordings, a small hose was glued to the nose and the animals were artificially respired (100-150 cycles/min). In these cases, anesthesia was additionally maintained by 50 % N<sub>2</sub>O and 50 % oxygen. We monitored the heart rate continuously and adjusted the depth of anesthesia to maintain a rate of 350-500 beats per minute. With the above procedures, we were able to optically record for about 20 h and electrically for up to 24 h.

### **II.1.2 Imaging and visual stimulation**

For visual stimulation we back-projected the stimuli with a video beamer onto a curved plastic screen covering the visual field in horizontal dimension from –50° to 120° measured relative to the vertical midline and between 20° below to 50° above the horizontal plane (with the head adjusted such that the mouth bar was positioned 3 mm below the inter-aural line). We stimulated at several positions in the visual field using moving square wave gratings, which changed their

orientations randomly every 0.6s (spatial frequency: 0.05 cycles/deg, speed: 2 cycles/second). These square shaped stimuli were presented in a random fashion at adjacent positions (for optical imaging: 7 columns and 3 rows of stimuli, 18° side length; for combined optical and electrical recording: 5 columns, 3 rows, 25° side length). Each six s stimulus presentation at one position was followed by a blank screen for eight s. To maximize the on-response we used minimal luminance (1.25 cd/m<sup>2</sup>; maximal luminance: 205 cd/m<sup>2</sup>) for blank screen and background intensity. In four experiments, computer-controlled shutters (Fig. 14) allowed independent stimulation of the ipsi- and contralateral eye. In all other experiments, we stimulated only the contralateral eye.

For optical imaging, the cortex was illuminated with monochromatic light of 707 nm wavelength. Images were captured using a cooled slow-scan CCD camera (ORA 2001, Optical Imaging, Germantown, NY), focused 700 μm below the cortical surface. Four “first-frames” (Bonhoeffer and Grinvald, 1996) and 10 frames of 600 ms duration were collected immediately before and during each six s stimulus presentation, respectively.

### **II.1.3 Electrophysiology**

In three animals, we extracellularly recorded single units after the optical imaging. The electrode recording sites were placed within area 17 previously determined by optical imaging. Using a similar stimulus as described above (5 columns, 3 rows, 25° side length) we recorded the spike response of 22 single cells discriminated by their waveforms (Brainware, Oxford, UK). Instead of randomizing orientation, we optimized for orientation, spatial frequency, and direction to elicit a maximal firing rate.

### **II.1.4 Analysis**

All images were “first frame-corrected”, i.e. from each image stack taken during presentation we subtracted the four “first frames” taken immediately before stimulus presentation. The resulting images were blank-corrected by subtracting the images acquired without stimulus from all images. In addition, the images were processed by a blood vessel extractor to remove blood vessel related artifacts. This method significantly improved the inter-trial correlation (Part III of this thesis). Twelve-bit digitized camera data were range-fitted such that for the single condition maps the 1 % or 3 % most responsive pixels (least responsive pixels) were set to black (white) for all DC-corrected or high-pass filtered images, respectively. Moreover, if not stated otherwise all images were DC-shift corrected by subtracting the mean from each single condition map. This correction is necessary because the mean background intensity can differ between single condition maps. To avoid erroneous DC correction due to large activated areas, which will

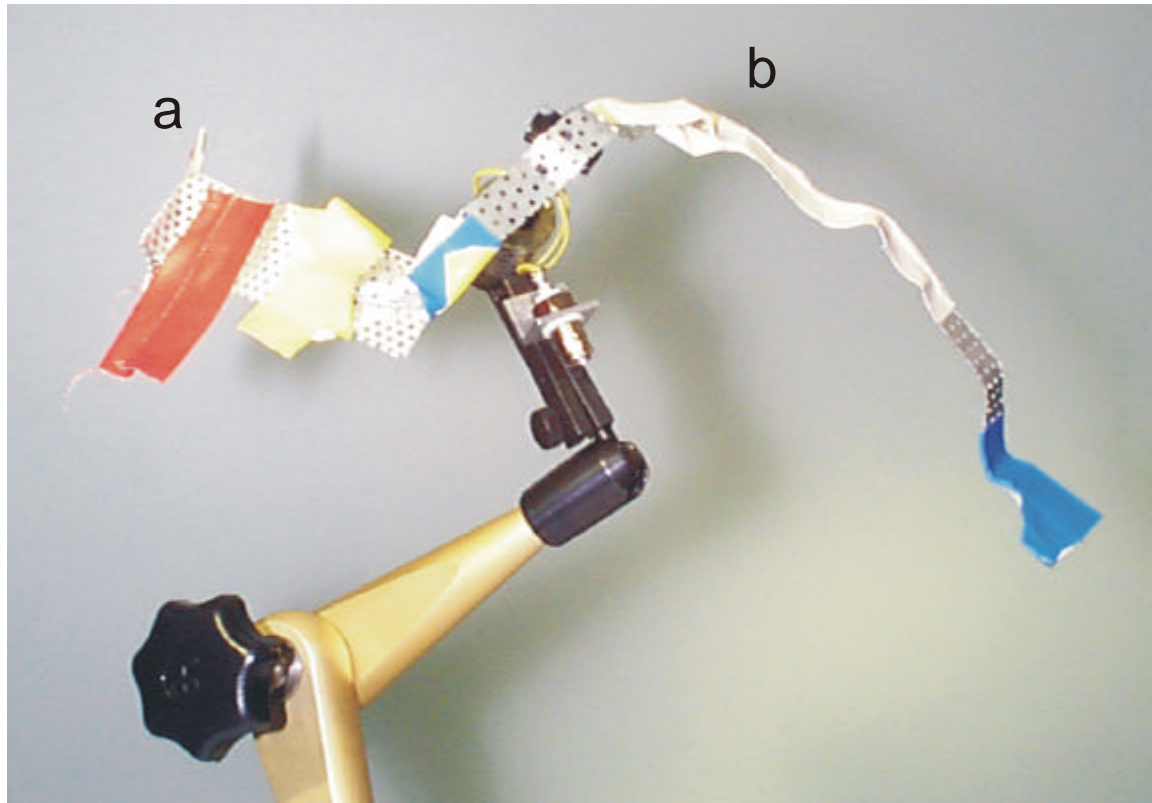


**Figure 14: Eye shutter for binocular stimulation. (a) The 700nm wavelength equipoise guarantees smooth eye occlusion supported by the extra-light anti-vibrator (b). The employed perforated high flex material was manufactured in cooperation with Swiss Cheese Inc. and Maerklin®**

slightly increase the mean of the intrinsic signal, we corrected for DC-shift in each image using the mean of only those pixels, which varied less than one standard deviation (SD) of the blank from its mean. Thereby, we excluded both potential patches and inhibitory surrounds from the DC-correction.

For quantification and alignment, all images were low-pass filtered with a Gaussian kernel of  $99\mu\text{m}$  half width. Since quantification requires a high signal-to-noise ratio we used 7(5) out of 11(9) animals with the best signal to noise ratio for the quantification with stimulation via the contra- (ipsi-) lateral eye.

The region of the primary visual cortex was determined by thresholding the maximum intensity projection of the intrinsic signal, i.e. the light absorption, five SD of the blank response above the mean of the blank. In some cases, the lateral area 18 had to be excluded by hand. The position of this lateral region could be easily delineated both by shape and by intensity. All subsequent processes were fully automated.

Both for averaging of single condition maps across animals and for quantification we aligned all sets of single condition maps imaged in different animals using the eight most prominent patches (corresponding to stimuli 2-5 in rows b and c, see Fig. 1a) elicited by visual stimulation as

reference points. The mean position of these patches determined the translation, and the mean of the angle of rows b and c the rotation required to bring maps from different animals into registry. To determine patch properties, we thresholded all maps 5 SD above the mean of the blank response. Patch position was then defined by the center of mass of the intrinsic signal in the primary visual cortex after thresholding the map. The cortical magnification factor (CMF) was determined by the mean distance to neighboring patches elicited by adjacent visual stimuli.

To visualize the overall retinotopic organization across the cortical surface, we color-coded visual field position in the following way: in the “peak position projection”, each pixel was assigned the color corresponding to the stimulus (Fig. 15a) eliciting the strongest response at this pixel. Because of this “winner takes all” algorithm, the peak position projection contains distinct borders between cortical regions responding preferentially to different stimuli. Whereas it is unlikely that the retinotopic position is mapped in such a discrete fashion in the visual cortex, this type of map is well suited to illustrate the retinotopic order. However, when patches activated by adjacent stimuli overlap extensively and when the intensity of the intrinsic signal differs between patches, this type of coding can lead to an erroneous representation of cortical retinotopy. To avoid this, we additionally employed the “average position projection”: in this coding scheme, we determine the average corresponding stimulus position at each pixel by computing the weighted mean across all stimuli eliciting an excitatory response (defined as intrinsic signal strength above the mean of the blank response). The color corresponding to the averaged stimulus position is assigned to this pixel.

To mask regions without a cortical response, color saturation was chosen to code for the maximum intensity projection of the intrinsic signal across all single condition maps for both the peak and the average position projection.

These coding schemes can be applied both to illustrate the retinotopic organization of the excitatory response as well as the pattern of surround inhibition. In the latter case, the projections are computed after inversion of the single condition maps.

### **II.1.5 Anatomy**

The size and shape of area 17 was determined in two animals after optical imaging using both SMI-32 antibodies (Sternberger Monoclonals, Lutherville, MD) and cytochrome oxidase staining as anatomical markers for area 17 (Duffy et al., 1998). To this end, the animal was euthanized and perfused with 0.1 M phosphate buffered saline (PBS) followed by 2 % paraformaldehyde in 0.1 M PBS. The brain was removed and postfixed for 1 hour. Then, the cortex was dissected and flattened, and 50  $\mu\text{m}$  tangential sections were cut on a freezing microtome. For alignment with the functional maps, the section containing the pial surface was cut at a thickness of 250  $\mu\text{m}$  to enable

the visualization of the superficial blood vessel pattern. Every other regular section as well as the thick section was stained for cytochrome oxidase according to procedures described by Wong-Riley (1979). The remaining sections were stained with the SMI-32 antibody following Duffy et al. (1998).

To compare the staining pattern with the imaged maps, we first aligned the superficial blood vessel pattern visible in the thick section with the blood vessel image taken before optical imaging (Bosking et al., 1997). Prominent blood vessels could be readily identified in both images, which were also used to correct for tissue shrinkage due to fixation. The thin sections were then aligned with the thick section using the pattern of vertical blood vessels, which was present in all sections. For display, the images of the stained sections were intensity clipped.

## **II.2 Results**

We imaged the intrinsic signal in mouse visual cortex evoked by stimulation at different positions in the visual field. To elicit a maximal cortical response, we presented a moving grating of changing orientations within a window of  $18 \times 18^\circ$  at each position. By using a curved screen, we were able to stimulate virtually the entire visual field of the mouse (see schematic in Fig. 15a).

Each single condition map corresponding to one retinotopic stimulus exhibit a prominent patch of activity, which is adjacent (and at the same time overlapping) with the primary patch corresponding to a visually adjacent stimulus (Fig. 15c), indicating that an ordered retinotopic map should be reconstructable from images recorded with this visual stimulation paradigm. The activity maps proved to be highly reproducible over the course of an experiment (Fig. 15d). The inter-trial correlation coefficient (0.71, 3 randomly picked animals) is comparable to the correlation coefficient for orientation preference maps in cat visual cortex (0.73, 3 animals), which can be regarded as a benchmark for optical imaging. This high inter-trial correlation also suggests that eye movements do not impede imaging of retinotopic maps.

### **II.2.1 Retinotopic organization of area 17**

Using stereotaxic coordinates as well as anatomical markers for area 17, we confirmed that the principal patches are located within the primary visual cortex. We determined the extent of area 17 with a maximum intensity projection of the intrinsic signal across all imaged single condition maps and aligned the resulting map with both cytochrome oxidase and SMI-32 (Duffy et al., 1998) stained sections using the superficial blood vessels as landmarks (Fig. 16, upper panels). Both, the size and the shape of the imaged and the stained area are in good agreement (Fig. 16, lower panels), indicating that the primary patches are located in area 17. Moreover, this correspondence suggests that the entire primary visual cortex is stimulated in our paradigm.

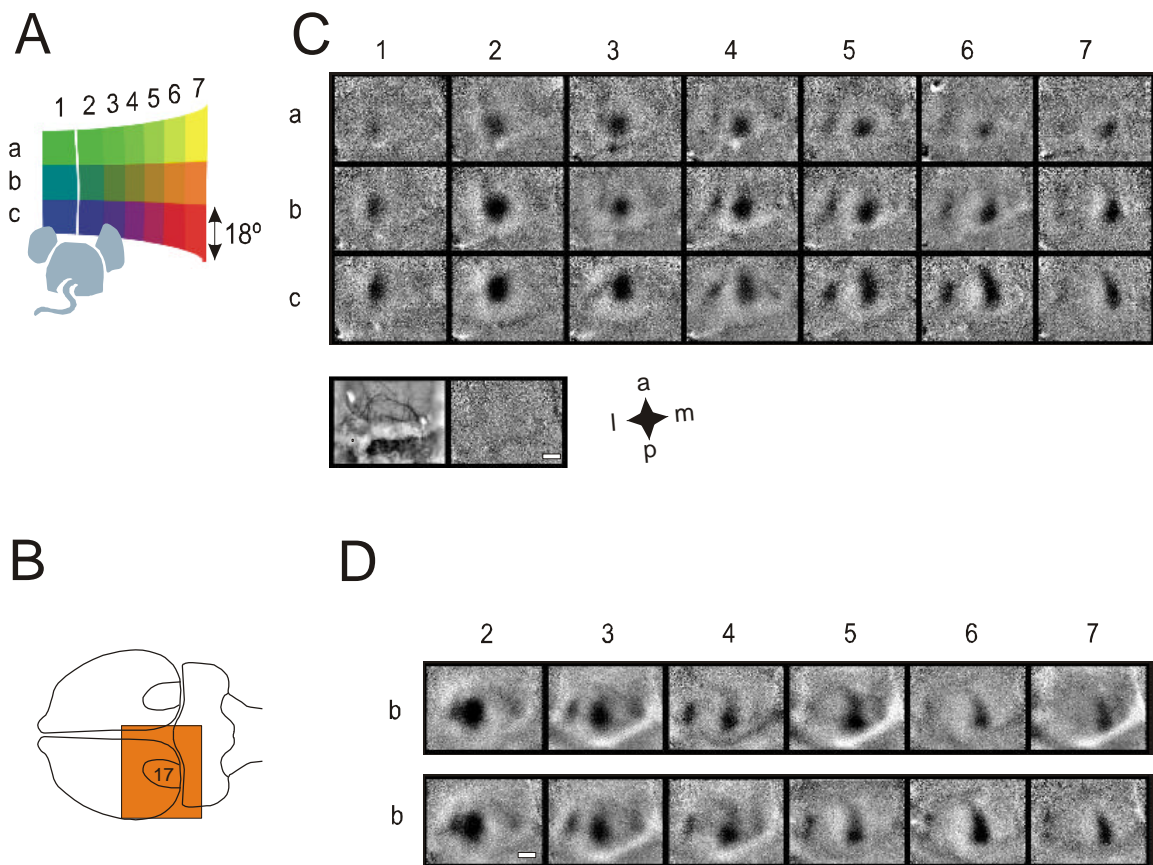


**Figure 15: Imaging cortical retinotopy in mice.** (A) For retinotopic stimulation, we used square-shaped windows of gratings ( $18^\circ$  side lengths) at adjacent positions within the visual field. The color code representing stimulus position was used to generate color-coded retinotopic maps. The white line indicates the vertical midline. (B) Schematic of the imaged cortical region as indicated by the orange window, which contains a rough outline of area 17. (C) Blank corrected single condition maps from one animal, with each map corresponding to a stimulus in (A), according to the indices. All maps are scaled and clipped equally. The blood vessel pattern imaged through the translucent skull is shown at the lower left. The map next to the blood vessel image displays the difference between images taken during two independent blank screen presentations. (D) Reproducibility of the imaged maps from a different animal. Both sets corresponding to stimuli b2-7 were averaged across 24 repetitions per stimulus imaged during subsequent blocks of data acquisition. Scale bars: 1mm.

To illustrate the overall organization of the entire retinotopic map, we employed a color code for stimulus position (Fig. 15a, 17). The color of each pixel within this map was assigned the color of the stimulus position, which had elicited the largest response at this point in the cortex (peak position projection, cf. Methods).

To mask cortical regions without activation, we used the maximum intensity projection of the intrinsic signal across all single condition maps for color saturation. Hence, non-responsive

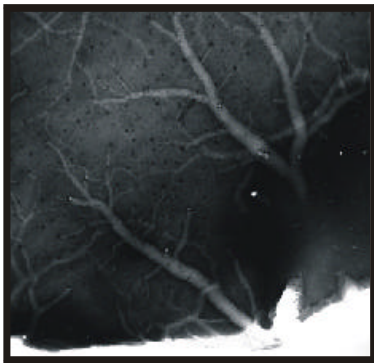
regions remain dark. Thereby, we obtain a multi-colored region in the center of the image, which exhibits a continuous retinotopic progression, both in vertical and horizontal directions.

As demonstrated by the correspondence between the maximum intensity projection of the intrinsic signal with the anatomical staining of area 17, this colored patch illustrates the retinotopic organization of the primary visual cortex. Although we also imaged activity in extrastriate areas, the intrinsic signal strength is much smaller in these regions. Therefore, extrastriate areas are not visible in this color-coded retinotopic map.

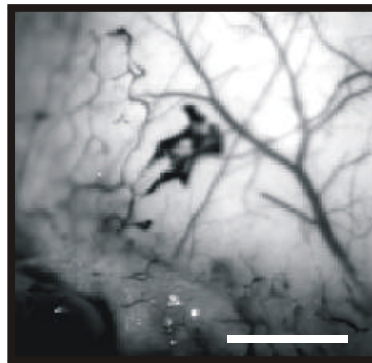
Since the retinotopic maps from different animals were very similar, we decided to average the single condition maps across animals. To this end, we first aligned maps from different animals using the center of mass of the eight strongest patches as reference points for translation and rotation. In addition, we standardized the experiments to control for variations in intrinsic signal strength, i.e., we set the mean across each image set to zero and the spatial SD to one.

## Anatomy

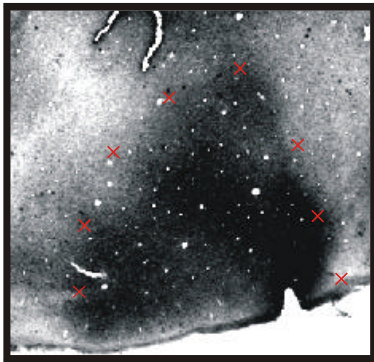
## Imaging



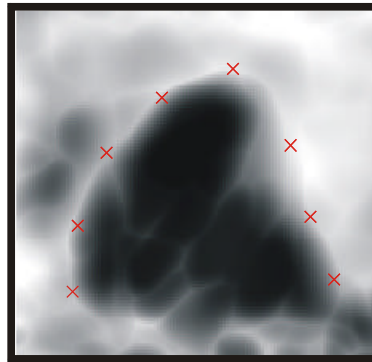
Blood Vessel Pattern



Blood Vessel Pattern



SMI-32 Staining



Activity Map

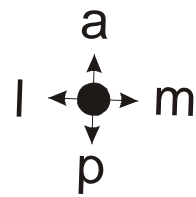


**Figure 16: Anatomical verification of imaging in the primary visual cortex. Superficial blood vessel patterns (upper panels) were used to align SMI-32 staining reflecting the anatomical position of area 17 (Duffy et al. 1998) with the maximum intensity projection of the intrinsic signal across all single condition maps. The red crosses were placed at the same positions in the staining pattern and the imaged map. Scale bar: 1mm.**

The resulting maps were then averaged across seven animals with the highest signal to noise ratio. Both, the averaged single condition maps (Fig. 18a) as well as the averaged color-coded retinotopic maps (Fig. 19a) are very similar to the data obtained from the individual animal presented in Figure 15. The possibility to reconstruct mouse retinotopy from the averaged single condition maps across animals indicates that both the variance due to the method as well as functional differences between animals are small.

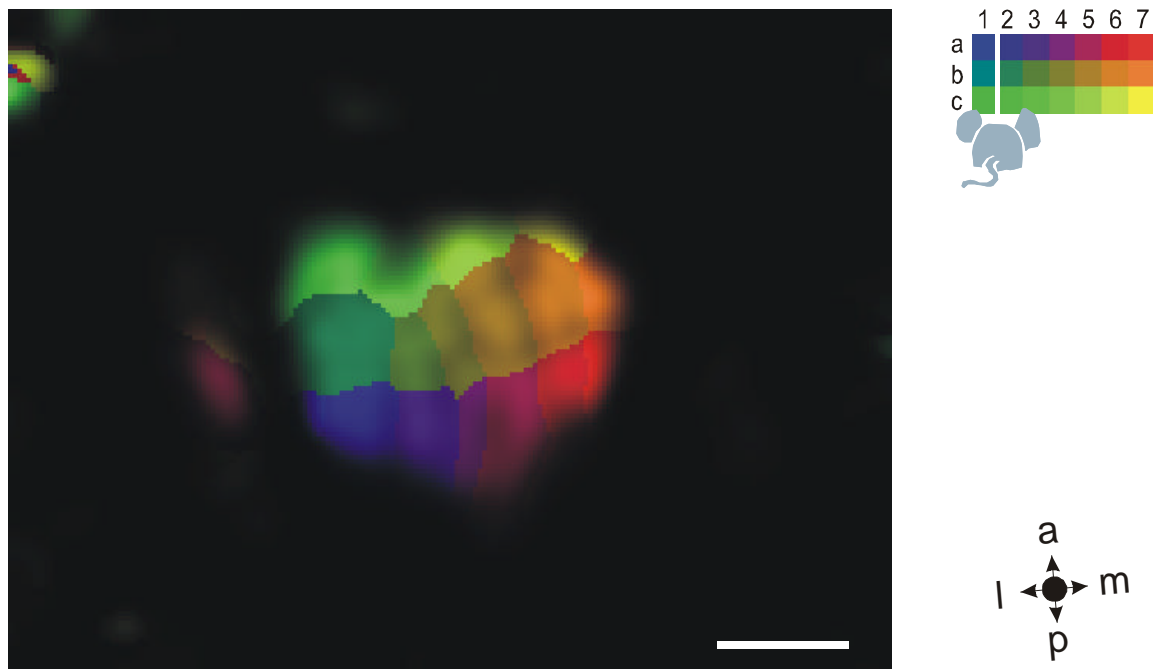


**Figure 17: Color-coded map of the overall retinotopic organization of area 17: the color of each pixel corresponds to the stimulus position, which elicited the strongest signal at this pixel. To mask out regions without cortical response, color saturation equals the maximum intensity projection of all single condition maps. Scale bar: 1mm.**

The low standard error of the mean of this averaging procedure (Fig. 18b) illustrates the high reproducibility per pixel. In addition, we quantified the inter-animal variability by computing the correlation coefficient between the single condition maps from different animals. The high correlation coefficient between maps from different animals ( $0.61 \pm 0.10$  SEM, 7 animals, 21 maps per animal) substantiates that the inter-individual variation between retinotopic maps is low.

To confirm the retinotopic maps obtained with optical imaging in the primary visual cortex, we recorded 22 single units in three animals using the same visual stimuli for optical and electrical recordings. The locations of the tracks within the functional maps were determined with the help of the superficial blood vessel pattern. The positions of the center of the receptive fields were defined by the stimulus causing the strongest response. The histogram of the distance between receptive field positions determined optically and electrically validates the retinotopic maps (Fig. 19b, plots per unit see Fig. 21a).

In summary, the imaged retinotopic order in the primary visual cortex, the high inter-trial and inter-animal correlation as well as the correspondence between electrical and optical recordings show that our paradigm is well suited to image the retinotopic map in mouse visual cortex.

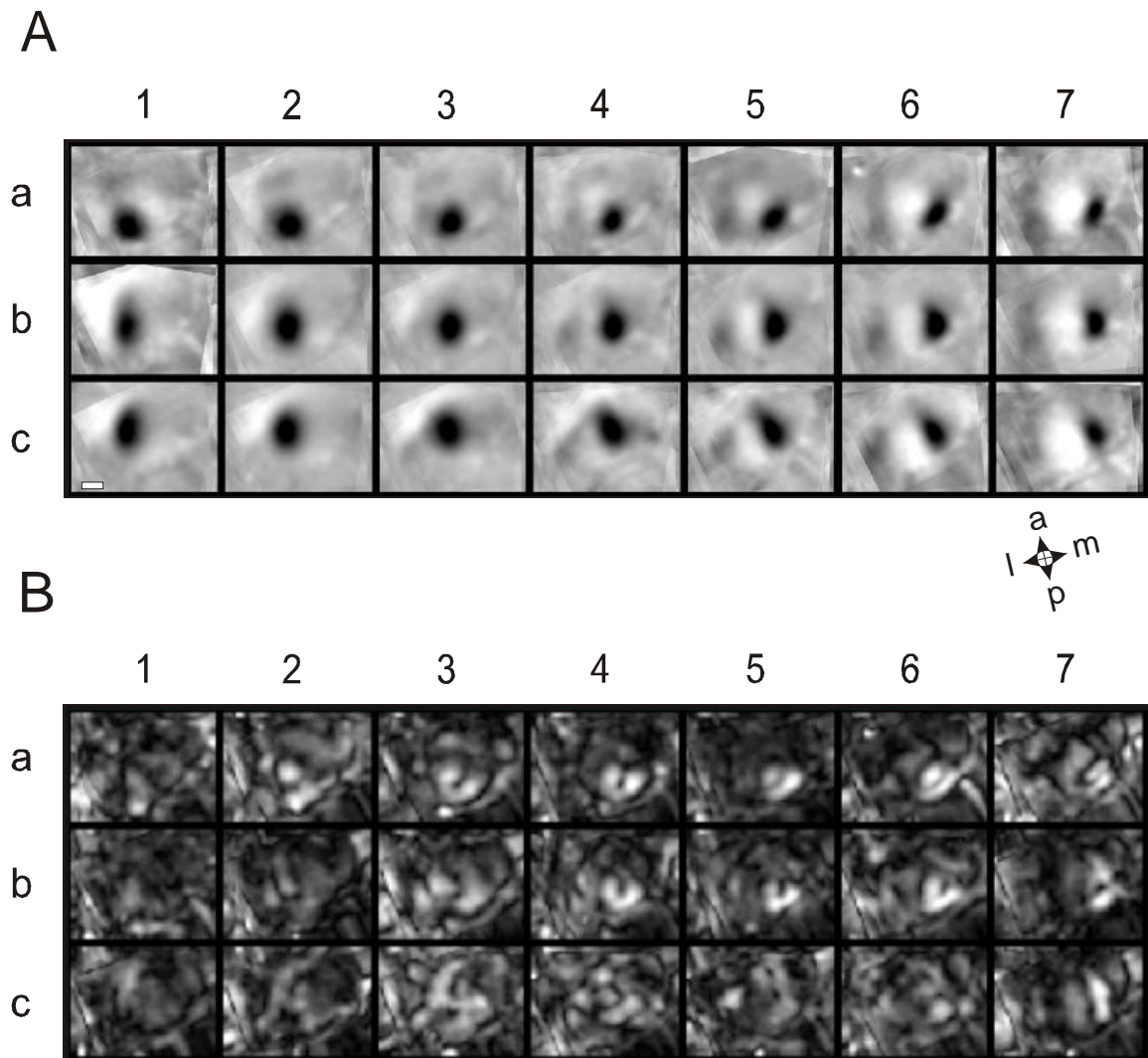


**Figure 18: Averaging maps across animals. (A) Single condition maps averaged across seven animals. Indices denote stimulus position according to Figure 15a. (B) Spatial distribution of the SEM for each map. For better visibility, the SEM maps are scaled by a factor of 5 in comparison to the single condition maps in (A). Scale bar: 1mm.**

## II.2.2 Cortical magnification factor

Having obtained the complete retinotopic map in area 17, we were able to measure the spatial distribution of the cortical magnification factor (CMF) in this area, a measurement, which is difficult to accomplish using conventional methods. For this purpose, we used the single condition maps from seven animals with the highest signal to noise ratio:

The CMF is defined as the scaling factor that relates a distance in the visual field (in degrees of visual angle) to the cortical distance (in mm) of the corresponding cortical representation (Daniel and Whitteridge, 1961). In our case, the reference length in the visual field is given by the center

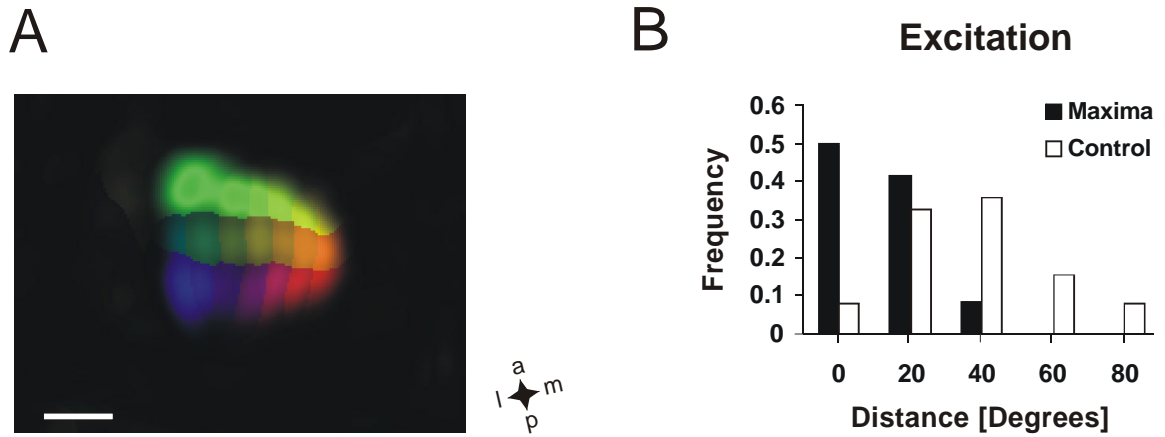


**Figure 19: (A) The color-coded retinotopic map based on the averaged single condition maps in Figure 18a. (B) Histogram of the distances between receptive field positions determined electrically and optically based on recordings from 22 neurons (black bars). The control distribution (white bars) was calculated from randomly assigning receptive field positions for 22 pairs and calculating the histogram of their distances. Note that 50 % of the electrically measured receptive field positions coincide with the optically determined position. Scale bar: 1mm.**

distance between two adjacent visual stimuli, i.e.  $18^\circ$ . The corresponding cortical distance was defined as the difference between the centers of mass of the activated patches in primary visual cortex corresponding to each stimulus. For this purpose, the single condition maps were thresholded five SD above the mean of the blank response.

The position plot (Fig. 20a) displays the positions of the centers of mass of each patch in area 17 for ipsi- and contralateral eye stimulation (green and red crosses, respectively), and confirms that the retinotopic organization across the entire primary visual cortex is maintained. Since the spacing of the visual stimuli is uniform, the CMF is directly proportional to the distance between positions, which correspond to adjacent visual stimuli.

Accordingly, we defined the horizontal and vertical CMF for a given stimulus position as the mean cortical distances corresponding to horizontal and vertical stimuli, respectively. To illustrate the distribution of the CMF across the visual field, we used a schematic of the stimulus pattern and assigned to each stimulus position the corresponding CMF, coded by lightness (Fig. 20b,c). Firstly, the position plot (Fig. 20a) indicates that the gradient of the CMF is relatively shallow in contrast to higher mammals such as primates. It varies only by about a factor of two. Moreover, it is obvious that the horizontal and the vertical CMF are different. While both the vertical and the horizontal CMF peak in the central visual field, the exact peak positions as well as the shape of the gradients do not match. Moreover, the vertical CMF is significantly larger than the horizontal CMF (vertical magnification:  $34.4 \pm 8.2 \mu\text{m}/^\circ$ , horizontal magnification:  $20.1 \pm 7.5 \mu\text{m}/^\circ$ ,  $p = 0.034$ , t-test,  $n = 7$ ).

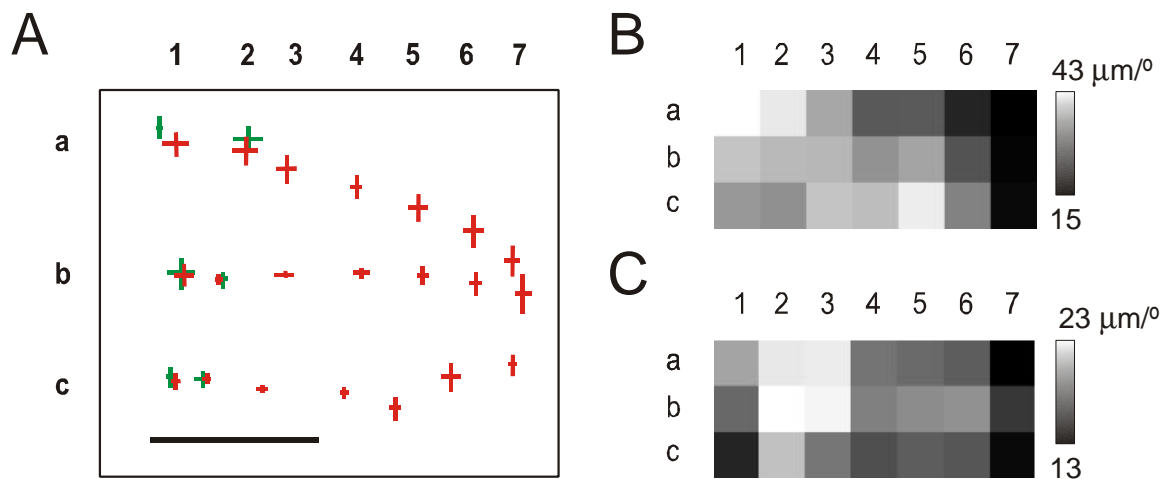


**Figure 20: Distribution of the cortical magnification factor (CMF) in area 17. (A) Positions of the centers of mass of the primary patches in area 17 averaged across seven animals. The lengths of the crossing bars indicate 1 SEM in vertical and horizontal direction. The red and green crosses correspond to stimulation of the contra- and ipsilateral eye, respectively. Numbers and letters denote column and row indices of the corresponding stimuli. Scale bar: 1mm. (B, C) Distribution of the CMF along the vertical (B) and horizontal (C) axes for each stimulus coded by lightness.**

The data presented above were obtained with monocular stimulation of the contralateral eye. In two animals, we also stimulated monocularly through the ipsilateral eye and compared the position of the cortical regions activated by either eye (Fig. 20a). As expected, only the two central columns of stimuli yielded a response after stimulating the ipsilateral eye. We found no significant differences between the patch positions for each stimulus when comparing ipsi- and contralateral eye stimulation for the two central columns of stimuli. ( $p = 0.19$ , t-test,  $n=5$ ). This indicates that the retinotopic order and exact position of the cortical projections driven by the ipsilateral eye correspond precisely to projections driven by the contralateral eye.

Alternating monocular stimulation of both eyes enabled us to compute ocular dominance maps in these animals. We failed to detect any clustering with respect to ocular dominance. Similarly, no clustering for orientation preference or selectivity, expanding stimuli, or on vs. off responses was detectable. This observation is in line with electrophysiological studies, which have provided at most weak evidence for the clustering of response properties in mouse visual cortex (Dräger, 1975; Mangini and Pearlman, 1980; Metin et al., 1988). Also, a recent comprehensive electrophysiological study in rat visual cortex failed to detect any clustering of orientation preferences (Girman et al., 1999).

### II.2.3 Lateral inhibition

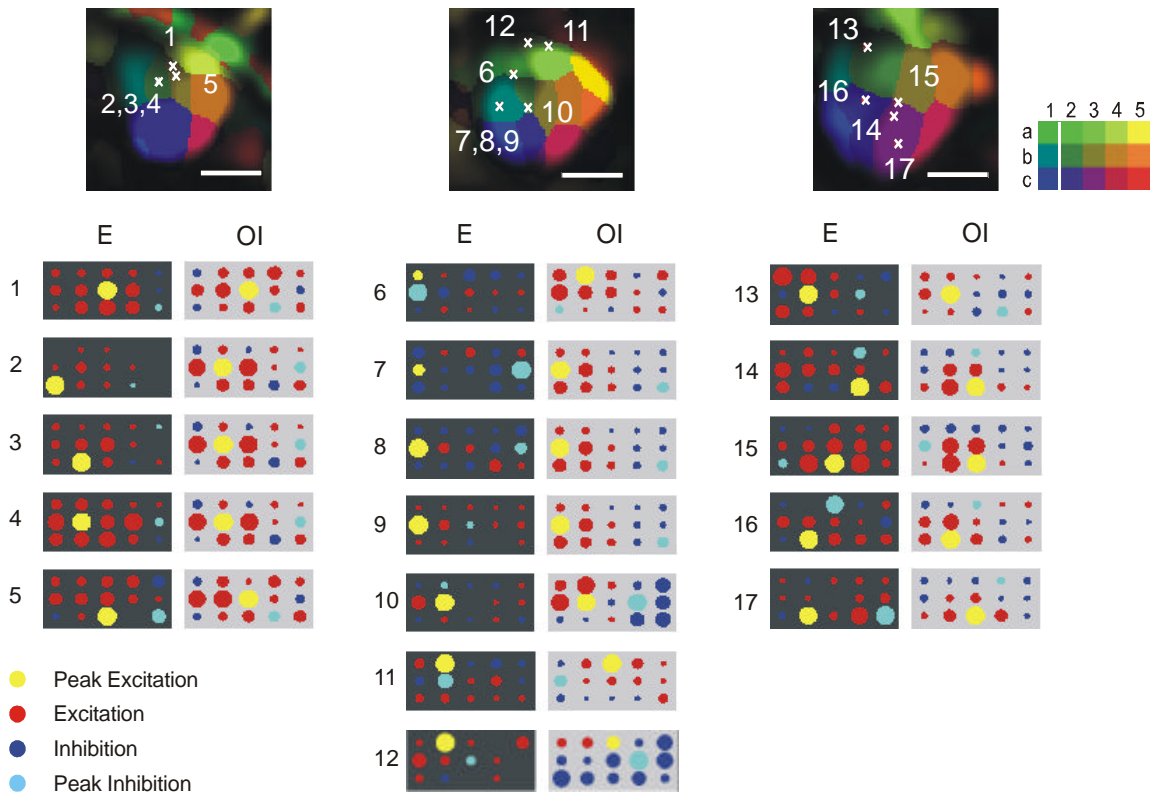
The single condition images (Fig. 15c) and the averaged maps (Fig. 18a) exhibit not only a principal dark patch, but also a light rim partly surrounding the dark patch. This increase in light reflectance, which corresponds to a reduction of the intrinsic signal below baseline, is particularly

pronounced for peripheral stimuli. This lighter surround region is not a filtering artifact, since the images have only been corrected for a DC-shift without any additional high-pass filtering. We hypothesized that this light surround region could be an optical correlate of lateral inhibition, which has been reported in single cell studies in mouse visual cortex (Dräger, 1975; Mangini and Pearlman, 1980; Simmons and Pearlman, 1982; Metin et al., 1988). To test this assumption, we recorded single units after optical imaging. A neuron was assigned an inhibitory surround if, during presentation of a grating at any position, its firing rate dropped below spontaneous levels recorded during presentation of the blank. According to this criterion the receptive fields of 17 out of 22 neurons recorded in the primary visual cortex exhibited an inhibitory surround. To compare the electrical and optical recordings, we measured the magnitude of the intrinsic signal within each single condition map at the cortical position of the electrode tracks. Similarly, a drop of the intrinsic signal strength below the blank response was taken as evidence for inhibition. We plotted the electrical and optical response by coding the firing rate or the amplitude of the intrinsic signal as the radius of circles corresponding to the different stimulus positions (Fig. 21a). For this analysis, only single units exhibiting lateral inhibition were chosen, an example of which is shown in Figure 21b: the raster plot illustrates the strong on-response for stimuli in the more central part of the visual field as well as the decrease in firing rate below baseline for stimuli in the peripheral visual field. The electrical and optical recordings exhibit very similar positions for the “receptive field centers” and the lateral inhibitory regions (Fig. 21a). We quantified this coincidence by comparing the distributions of the distances between the electrically and optically determined positions with a randomized control. The vast majority (83 %) of the distances between electrically and optically determined receptive field centers are at most 20° in visual space apart from each other. For inhibition, 59 % of the positions of the strongest inhibition are maximally 20° in visual space apart from each other (Fig. 22a). It is to be expected that the coincidence of the inhibitory peaks is lower than the correlation of the centers of the receptive fields, because the inhibitory surround is more broadly spread out than the excitatory patches and because it has a lower signal to noise ratio. Moreover, note that in the case of inhibition fewer pairs fall into the 0°-distance bin in comparison to the 20°-distance bin.

Such a shape of the distance histogram is to be expected because the alignment of the two recordings introduces noise. Since the probability of hitting adjacent positions is roughly three fold higher than complete coincidence (cf. control distribution), this bias towards the 20°-distance bin is not surprising. The observed correlation between the decrease in the intrinsic signal and the electrically recorded lateral inhibition provides strong evidence that the intrinsic optical signal is a monotonous function of the firing rate. Therefore, a drop of the intrinsic signal below baseline indicates neuronal inhibition. To illustrate the spatial organization of the inhibitory surround, we

constructed a color-coded inhibition map. To this end, we employed a similar algorithm as for the color-coded retinotopic map (Fig. 17).

A



B

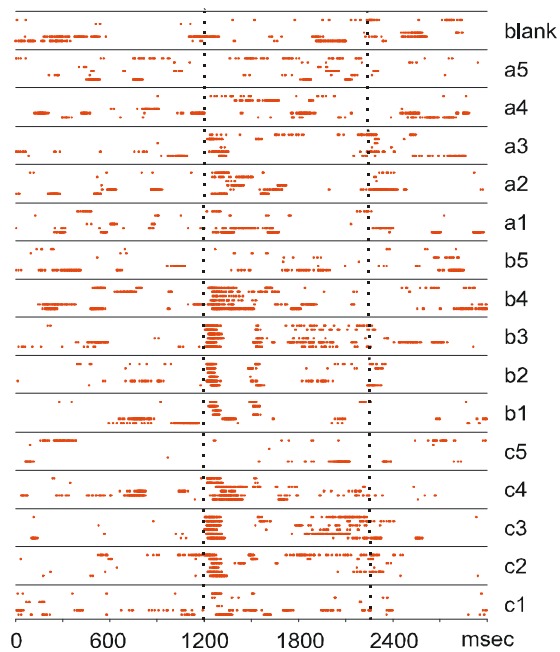


**Figure 21: Optical and electrical recordings of lateral inhibition.** (A) 2d-plot of position tuning curves recorded electrically (dark gray background) and optically at the positions of the electrode tracks (light gray background). Data are from 17 neurons in three animals. Each circle displays the response to the corresponding stimulus position. The radius of each circle is proportional to the absolute value of the normalized firing rate or the position-tuning curve reconstructed from the optical signal at the track position. Red (blue) color indicates supra (sub) blank response. The circle corresponding to the stimulus, which elicits maximal (minimal) response, is colored in yellow (turquoise), see also legend at lower left of panel. In the top row the track, positions are marked in the color-coded retinotopic map of the respective animal. Scale bars: 1mm. Color code for stimulus position used for experiments with combined electrical and optical recordings presented at upper left of panel (A). (B) Raster dot diagram of cell #1 responding preferentially to stimulus b3. Vertical broken lines indicate stimulus on- and offset. Note the strong on-response as well as the drop in firing rate below baseline for stimulus condition c5.

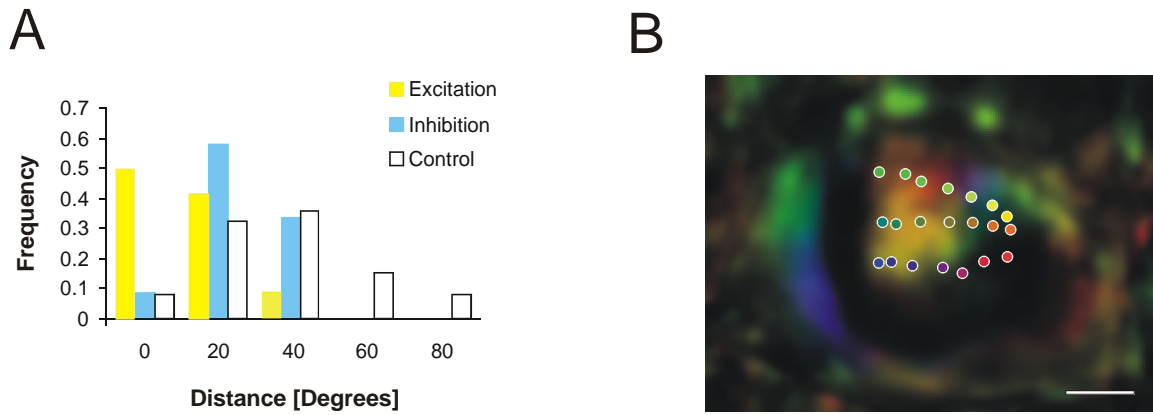


**Figure 22: (A) Histogram of the distances between the positions of the peaks of excitation (yellow bars,  $n = 22$ ) and inhibition (turquoise bars,  $n = 17$ ) determined electrically and optically. Control distribution (white bars) constructed from randomized pairs of positions. (B) Color-coded inhibition map of the averaged single condition maps. Pixel color denotes the mean across all stimuli eliciting inhibition. The minimum intensity projection of all single condition maps codes for color saturation. The positions of the primary excitatory patches in area 17 are marked by circles, with the corresponding stimulus color (cf. Figure 20a). Comparing the retinotopic position with the pattern of inhibition illustrates the systematic pattern of surround inhibition: the inhibition for a given stimulus peaks approximately at a cortical position representing the visual field  $60^\circ$  away from this stimulus. Scale bar: 1mm.**

However, instead of using the peak position projection as a color code, we used the average position projection (see Methods) and applied it to the inverted averaged single condition maps (Fig. 22a). In this map, color saturation codes for the minimum intensity projection of the intrinsic signal, implying that regions, which are strongly inhibited, appear in bright color. The average position projection was better suited to illustrate the less well-ordered topography of surround inhibition. It is more informative about the actual distribution of inhibition because inhibition evoked by different stimuli differs more strongly in intensity of the intrinsic signal and overlaps to a greater extent than excitation.

The positions of the principal excitatory patches corresponding to each stimulus are overlaid on the map shown in Figure 22b to compare the retinotopic order with the pattern of surround inhibition. This map illustrates the fixed relationship between excitation and inhibition. On average, the mean across all local minima within the inhibitory surround is  $56 \pm 11^\circ$  (SD,  $n = 7$ ) away from the excitatory peak, expressed in visual field coordinates. Both, the small standard deviation as well as the possibility to reconstruct the ordered inhibition map from the averaged single condition maps suggests that also the “retinotopic” map of inhibition is well preserved across animals.

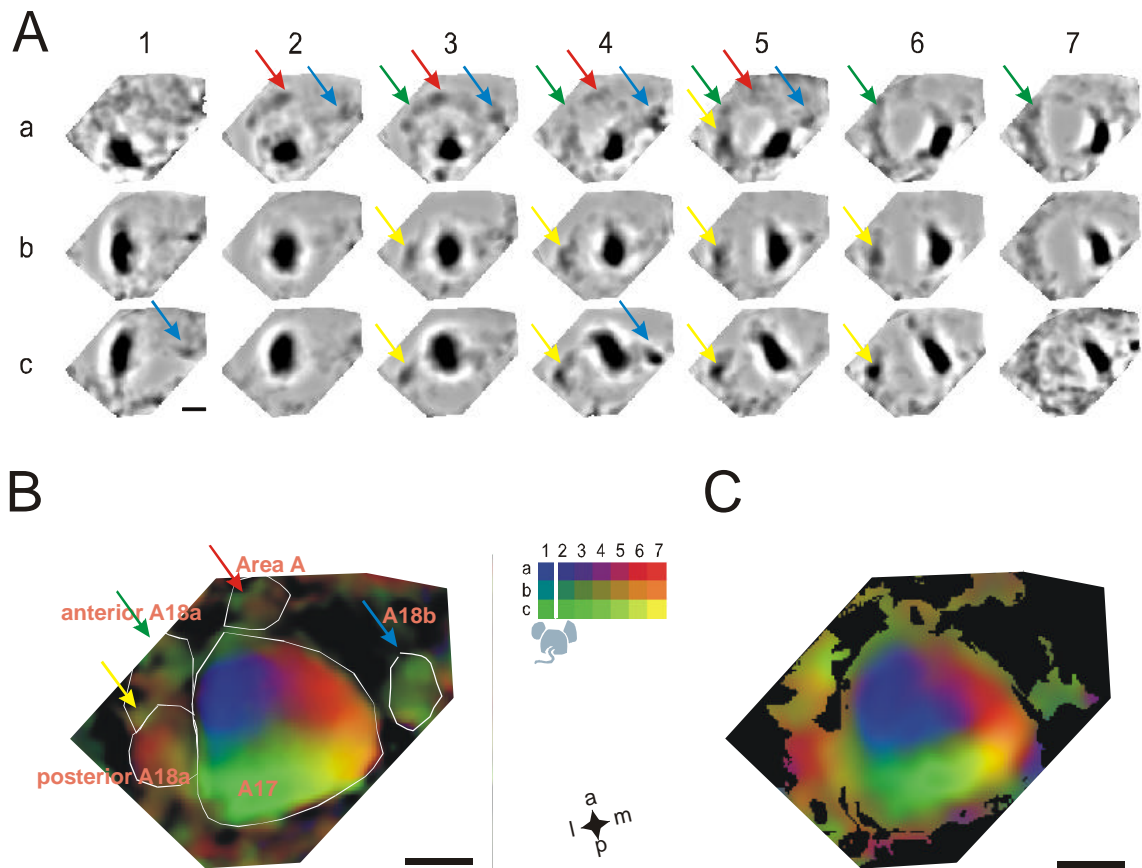


**Figure 23: Retinotopic organization of extrastriate visual areas.** (A) High-pass filtered, averaged single condition maps (boxcar = 800 mm, n=7). The colored arrows were placed at the same positions in all maps; they indicate distinct patches in extrastriate areas (yellow arrows: anterior area 18a; green: posterior area 18a; red: area anterior; blue: area 18b). Note that in many images several extrastriate patches are visible. (B) Color-coded retinotopic map using the high-pass filtered single condition maps shown in (A). The color corresponds to the code for the average position projection. Color saturation is proportional to the scaled maximum intensity projection of the high-pass filtered maps. Candidate extrastriate areas were outlined based on the presence of separate patches in the single condition maps in (A); (C) Color-coded retinotopic map with the color saturation of all regions with higher (lower) intrinsic signal than 2 SEM set to maximum (minimum). Scale bars: 1mm.

## II.2.4 Extrastriate cortical areas

We found that in addition to the strong response in the primary visual cortex, smaller patches are visible in extrastriate cortical areas in the single condition images (cf. Fig. 15b). Since the strong response within the primary visual cortex tends to overshadow these additional patches, we used a strong high-pass filter to reveal peaks of lower intensity and smaller size in the averaged single condition maps (Fig. 23a).

Lateral, anterior, and medial to area 17 small patches are visible in several of the single condition maps. Colored arrows in the maps in Figure 23a indicate the positions of several of these patches.

Note that patches in extrastriate areas are visible in only some of the single condition maps, indicating that in these areas only a portion of the visual field is represented. Again, we color-coded retinotopic position using the high-pass filtered single condition maps. To avoid overshadowing of extrastriate areas by the strong response in area 17, we scaled the maximum intensity projection appropriately (Fig. 23b).

Since, as for inhibition, the intrinsic signal differed markedly between patches evoked by adjacent stimuli and due to the large overlap of patches in extrastriate areas, we coded color by the average position projection rather than the peak position (see Methods). To provide a statistical estimate of the validity of this map, we masked out all regions where the intrinsic signal was below two SEM calculated across animals and set the color saturation to its maximum in the remaining regions (Fig. 23c). This map illustrates that virtually only in the outlined extrastriate areas a significant visual response can be recorded.

The color-coded retinotopic maps in Figure 23b,c suggest that lateral to area 17, in a region probably corresponding to the posterior part of area 18a (Caviness, 1975), one retinotopically-organized area is located (yellow arrows). In this area, the lateral part responds to peripheral stimuli, while the medial part is activated by central stimuli, i.e. the representation in posterior area 18a seems to be mirrored at the border to area 17 with respect to the representation in the primary visual cortex as in other animals (Van Essen, 1979).

From the single condition maps, we infer the existence of a distinct area in the anterior part of area 18a (green arrows) as well as an area anterior to the primary visual cortex (red arrows), which may be homologous to area A described in rats (Lewis and Olavarria, 1995).

We propose that these regions are separate areas, because distinct patches corresponding to each region can be observed in the same single condition maps. In addition, medial to area 17 – a region that has been termed area 18b (Caviness, 1975), we observed non-retinotopically organized visual activity (blue arrows). While the posterior part of area 18a exhibited a retinotopic order, in all other areas, we failed to detect clear retinotopic patterns. These three non-retinotopically organized regions respond preferentially to stimuli in the upper part of the visual field, while the posterior part of area 18a contains mainly a representation of the lower visual field.

## II.3 Discussion

We have employed optical imaging of intrinsic signals to visualize the retinotopic organization of mouse visual cortex. The resulting single condition maps are highly reproducible and demonstrate that retinotopy is maintained across the entire mouse primary visual cortex. In addition, we observed visually evoked activity in several extrastriate areas. The optically determined maps

were confirmed with single unit recordings, which provided independent evidence for the presence of inhibitory surrounds seen in the imaged maps.

### **II.3.1 Averaging the intrinsic signal across animals**

Optical imaging of intrinsic signals is based on extensive averaging across multiple trials in individual animals (Grinvald et al., 1986). Since most of the columnar structures, which are routinely imaged in the visual cortex of higher mammals, e.g. orientation or ocular dominance columns, are variable from animal to animal, averaging across animals is impractical for these maps. In contrast, the arrangement and the layout of the retinotopic map seem to be rather stable between animals from the same species (Dräger, 1975; Tusa et al., 1978; Wagor et al., 1980; Tootell et al., 1988). In fact, we found a high inter-animal correlation of aligned single condition maps, thus we could reconstruct retinotopy from the directly averaged maps between animals. We believe that this approach is the most efficient and illustrative way to display data from multiple animals. In particular, one can directly estimate the inter-animal variability of the maps by the corresponding distribution of the inter-animal standard error of the mean per pixel. In addition, averaging maps across animals provides a very intuitive way to illustrate properties, for which automated quantification within the single condition maps is difficult. In this study, this advantage has proven very useful for analyzing the retinotopic structure of extrastriate areas, which would have been very difficult in individual animals. Obviously, low inter-animal variability is a prerequisite for reconstruction of ordered maps using the averaged single condition maps. Potentially, for optical imaging within the barrel cortex this approach might be very useful.

### **II.3.2 Inter-ocular alignment of retinotopic maps**

By stimulating the ipsi- and contralateral eye independently, we were able to study the organization of ocular preference in mouse visual cortex. We failed to detect any pattern of regions responding preferentially to one eye implying that unlike higher mammals ocular dominance is not mapped in a parcellated fashion across mouse visual cortex. Furthermore, we found that the retinotopic maps recorded during stimulation of each eye matched almost completely. This suggests that the retinotopic projections are well aligned between the eyes. Since this alignment could be measured with high precision, optical imaging of mouse visual cortex provides a promising tool to clarify the developmental mechanism generating this inter-ocular match.

### **II.3.3 Cortical magnification factor and ganglion cell density**

It has been hypothesized that the primary central representation of sensory systems scales with the receptor surface (Talbot and Marshal, 1941; Hallett, 1987), i.e. that the distribution of the cell number across the sensory surface matches the distribution of the cell number or area of its neuronal representation. The favorite model to test this hypothesis is the relation between the distribution of the retinal ganglion cell density and the corresponding magnification factor in cortical or subcortical structures. All these studies have been performed in higher mammals, which have a fovea or a similar retinal specialization and which were found to display a corresponding increase in magnification factor at the foveal representation. Some studies (cortex: Wässle et al., (1989); superior colliculus: Mark et al., (1993), Rosa and Schmid, (1995)) supported the scaling hypothesis, while others obtained contradicting results (cortex: Azzopardi and Cowey (1993); superior colliculus: Berson and Stean, (1995) Quevedo et al., (1996)). Despite the conflicting evidence regarding the match between the distributions of retinal ganglion cell density and area of the neural representation, the peaks of the distributions did coincide. Mice provide an interesting model to study the scaling hypothesis, since retinal ganglion cell density peaks in the periphery (Dräger and Olsen, 1981), rather than centrally. However, in animals with a small visual cortex such as mice, it is difficult to derive the CMF from electrical recordings. In contrast, as we have shown, optical recordings are well suited to accurately measure both the horizontal and vertical CMF. Our optical data indicates that in mice area 17 the peaks of the vertical and the horizontal CMF do not coincide with the peak in retinal ganglion cell density. Thence, we conclude that in mice primary visual cortex, the neural representation of the visual field does not scale with retinal ganglion cell density.

### **II.3.4 Optical imaging of inhibition**

The intrinsic signal recorded in optical imaging has been shown to be a metabolic correlate of neural excitatory activity (Grinvald et al., 1986; Frostig et al., 1990). However, it is unclear, to which degree this signal also correlates with decreases in neural firing rate below baseline. In studies using related metabolic signals, no conclusive correlation between inhibitory activity and either 2-deoxyglucose mapping (Ackermann et al., 1984; Sharp et al., 1988) or functional magnetic resonance imaging (Waldvogel et al., 2000) could be established.

In mouse visual cortex it has been shown with extracellular recordings (Mangini and Pearlman, 1980; Simmons and Pearlman, 1983), that visual stimuli elicit lateral inhibition. We were able to image a correlate of this lateral inhibition: in the single condition maps, a downward deflection of the intrinsic signal surrounds the activated cortical region in a pattern, which is consistent across different animals. Using single cell recordings, we confirmed that decreases in neuronal firing rate

below baseline correlates with decreases of the intrinsic signal. Thus, optical imaging is capable of visualizing the effect of neuronal inhibition.

Does this correlation hold true for other metabolic brain imaging methods as well? Since we imaged the intrinsic signal at a wavelength of 707 nm, the relative contribution of the light scattering component is most likely higher than the oxymetry component (Malonek and Grinvald, 1996). This raises the possibility that the decrease in intrinsic signal in this case is not caused by changes in a true metabolic signal but rather in light scattering. Therefore, 2-deoxyglucose mapping as well as functional magnetic resonance imaging based on the oxymetry component, might fail to detect this decrease. In any case, lateral inhibition in mouse visual cortex might serve as a model system to further elucidate the differential contributions of the intrinsic signal components associated with inhibition. In addition, optical imaging of inhibition in mice could further our conception of the development and structure of inhibitory circuitry.

### **II.3.5 Extrastriate areas**

Previous electrical recording and tracing studies have been contradictory with respect to the number and structure of extrastriate visual areas in mice. With either method, it is difficult to reconstruct the retinotopic structure of a visual area from the data, because only a relatively small number of cells or traced connections can be gathered from a single mouse. Hence, data from many animals has to be aligned using gross anatomical landmarks or stereotaxic coordinates rather than physiological reference points. Moreover, reconstruction of the complete retinotopic map usually requires interpolation from a relatively sparse data set. Using optical imaging, we were able to map retinotopy in the entire visual cortex across the complete visual field within individual animals. The high reproducibility of these maps made it feasible to use functional landmarks to align data from several animals. Moreover, we could provide statistical confidence intervals for the averaged retinotopic maps.

In the region lateral to area 17, usually referred to as area 18a (Caviness, 1975), we found two visual areas. The same result has been reported in the very comprehensive electrophysiological study by Wagor and colleagues (1980), see also (Dräger, 1975). We found a retinotopic representation only in the posterior part of area 18a; the anterior part does not exhibit any detectable retinotopic order.

In addition, we found a distinct area anterior to area 17, which has not been described in previous mouse studies (Wagor et al., 1980; Dräger, 1975), however, it has been identified in some anatomical studies of rat visual cortex (Simmons et al., 1982; Coogan and Burkhalter, 1993; Lewis and Olavarria, 1995). We also observed a visually responsive area medial to area 17,

commonly called area 18b (Dräger, 1975; Caviness, 1975; Wagor et al., 1980), which lacked an obvious retinotopic organization.

It is difficult to compare our results with data from other rodents like the rat, since no consensus on the number of extrastriate areas has been reached there, either. While some authors report more than four areas in the rat (Espinoza and Thomas, 1983; Montero, 1993), others claim that only one or two extrastriate visual areas exist (Cusick and Lund, 1981; Malach, 1989; Rumberger et al., 2001). In pilot studies, we have successfully used optical imaging to map the retinotopic structure of the primary visual cortex in rats (Schuett et al., 2000). Perhaps an optical imaging approach might also be useful to determine the number and organization of extrastriate areas in rats and other small mammals. Since our results strongly suggest that at least four extrastriate visual areas are present in mouse visual cortex, we assume that a similar complexity is to be found in larger rodents.

### **II.3.6 Imaging mouse retinotopy as a tool for the study of transgenic animals**

Genetically altered mice have become a standard tool to assess the function of different proteins in the mammalian nervous system. It is by now well established that gradients of certain probes such as ephrins are instrumental in setting up a retinotopic map (Baier and Bonhoeffer, 1992; Cheng and Flanagan, 1994; Drescher et al., 1995). Imaging mouse retinotopy now provides a tool to functionally assess retinotopic maps in such genetically altered mice. There are a number of aspects, which are of great advantage for such investigations. Firstly, the small inter-animal variance of the intrinsic signal is very helpful for this approach because averaging maps across animals provides a tool to detect even subtle differences between experimental groups. In particular, the possibility to statistically test the optic response per pixel across animals might help to substantiate such differences. Since the position of excitatory patches and the corresponding CMF can be quantified with high precision, these measures are ideally suited for studying the formation of topographic maps in genetically altered mice. Finally, as we have shown, optical imaging provides an efficient tool to map extrastriate visual areas in the mouse. Thus, genetic factors influencing areal specification in the cerebral cortex can be investigated easily.

### **Part III    Extraction of blood vessel related artifacts from optical imaging data**

Optical imaging of intrinsic signals has been successfully employed to map the functional architecture at high spatial resolution in different sensory systems (Grinvald et al., 1986; Bonhoeffer and Grinvald, 1991; Blasdel, 1992; Masino et al., 1993; Bonhoeffer and Grinvald, 1996; Rubin and Katz, 1999; Antonini et al., 1999). Two components of the intrinsic signal have a relatively high spatial resolution and thus allow for the visualization of columnar structures in the cerebral cortex: the oxymetry component caused by light reflectance changes due to an increase of the deoxy-hemoglobin/oxy-hemoglobin ratio after the onset of neural activity and the light scattering component, which results from a non-blood related increase in light absorption in regions of increased neural activity (Frostig et al., 1990; MacVicar and Hochman, 1991; Bonhoeffer and Grinvald, 1996; Malonek et al., 1997; Malonek and Grinvald, 1997). In contrast, the blood volume component of the intrinsic signal, which is caused by activity related increases in blood flow and ongoing hemodynamic changes, is considered a major noise source in high-resolution optical imaging (Grinvald et al., 1986; Mayhew et al., 1996; Chen-Bee et al., 1996; Malonek and Grinvald, 1997; Vanzetta and Grinvald, 1999). Since the latter component is much stronger than the high-resolution components (Malonek and Grinvald, 1996), signal to noise levels are rather low in typical optical imaging experiments and thus require prolonged stimulation and extensive averaging.

Despite these limitations, in several systems like cat or monkey visual cortex, columnar structures can be resolved routinely with high reproducibility. In rodents, however, reproducible imaging is more difficult because of the smaller signal to noise level. While the reasons for this are not entirely clear, the high metabolic rate of these smaller animals and the relatively large blood vessels on the surface of the lissencephalic cortex are likely to contribute to the pronounced hemodynamic noise. A number of analysis methods have been employed to improve the signal to noise ratio to allow imaging in systems with such large hemodynamic noise. Principal component analysis (Cannestra et al., 1996), the indicator function approach (Everson et al., 1997; Gabbay et al., 2000), as well as extended spatial decorrelation (Stetter et al., 2000) have been applied to optical imaging data for this purpose. All these methods do not directly identify the hemodynamic noise but rely on either significance testing or the known time course of the signal to improve optical imaging data. To extract hemodynamic noise more effectively and thus facilitate

reproducible optical imaging in rodents, we have developed a signal analysis technique to extract artifacts caused by large blood vessels. This so-called blood vessel extractor (BVE) exploits fluctuations within the intrinsic signal while no stimulus is present. By using the correlation of these fluctuations with the actual blood vessel pattern, fluctuation components are selected, which are most likely to contain blood vessel related artifacts. These fluctuation components are extracted from the raw single condition maps typically recorded with optical imaging. This technique increases the reproducibility of optical imaging in cat, mouse, and rat visual cortex, and it reduces the overall data acquisition time because less averaging is needed to obtain high quality maps.

## **III.1 Methods**

### **III.1.1 Surgery and optical imaging**

In 8-12 week old kittens anesthesia was induced with an i.m. injection of ketamine (20–40 mg per kg) and xylazine (2–4 mg per kg). Animals were tracheotomized and artificially ventilated (60 % N<sub>2</sub>O, 40 % O<sub>2</sub>, 0.7-1.0 % halothane). ECG, EEG, end-tidal CO<sub>2</sub> and rectal temperature were monitored continuously. The animals were relaxed with gallamine triethiodide (Sigma, 10 mg/h) to prevent eye movements and to ease artificial ventilation. The skull was trepanated over area 17 or 18 and the dura was removed. Agar flattened by a cover glass was used to stabilize the cortex. Maps of orientation preference in area 17 were obtained by stimulation with moving whole field gratings. In one presented example (Fig. 24), we also used a stimulus configuration, where a circle (12° diameter) containing a moving grating of one orientation was presented at various retinotopic positions.

Long Evans rats (8-14 week) and Black 6 mice (6-14 week) were anaesthetized with a combination of urethane und ketamine (initial anesthesia 2–4 mg/kg ketamine, 10 mg/kg Urethane, maintained by i.p. infusion: 2 mg/kg ketamine, 2 mg/kg urethane). For rats, the skull was opened and the dura was left intact. The cortex was stabilized with agar flattened by a cover glass. In mice, the bone was not opened but made transparent with silicon oil. As visual stimuli, square windows (18° x 18°) containing moving gratings of randomly changing orientations were presented at several positions within the visual field (cf. Part II of this thesis).

For optical imaging, the cortex was illuminated with light of 707 nm. Images were captured using a cooled slow-scan CCD camera (ORA 2001, Optical Imaging, Germantown, NY), focused 700 mm below the cortical surface. Four first frames (Bonhoeffer and Grinvald, 1996) and 10 frames of 600 ms duration were collected during each 6 s stimulus presentation, followed by a 9 s inter-stimulus interval during which either the next stimulus was presented stationary (cats) or a blank

screen was shown (rats and mice). We found that the application of the BVE is particularly useful in combination with this relatively long stimulation and recording time, since the BVE strongly reduces the contribution of the long-latency blood volume component, thus leading to an overall better image quality in comparison to shorter exposure times.

Analysis: images were blank (mice and rat) or cocktail blank (cat) corrected. While high quality images from cat and mice are unfiltered, for the lower quality rat images we used a Gaussian filter of 50 x 50 mm. For the computation of the correlation coefficients between subsequent trials, all images were sigma-filtered using a threshold of one standard deviation of the neighboring pixels iterated for 20 times to remove pixel noise. We determined the stimulated cortical region by thresholding a minimum intensity projection of all extensively averaged single condition maps (more than 4 trials, one trial consists of 6 repetitions of the randomized sequence of stimuli.) two standard deviations of the mean above the mean of the blank response.

### **III.1.2 Blood Vessel Extractor**

To extract noise caused by hemodynamic fluctuations it is necessary to firstly determine these fluctuations and secondly extract them according to a noise-minimizing optimization criterion. Figure 24 illustrates the principle algorithm of the BVE, which implements these two steps.

#### **III.1.2.1 Determination of fluctuations**

To compute the intrinsic signal fluctuations a sequence of images obtained without stimulus presentation was taken interleaved with the normal stimulus presentation. In addition to this blank sequence, the so-called first frames taken before the presentation of each individual stimulus were also used for the following analysis. To reveal fast fluctuations of the signal, the blank sequence is temporally high-pass filtered. We have implemented this filter by subtracting subsequent images from each other. To avoid redundant extraction and to limit the number of components used for extraction, we perform a principal component analysis across the difference image stack. Principal component analysis linearly maps the difference image stack onto a new orthogonal set of images, which is ordered according to their variance, i.e. signal strength. We then select only those fluctuation images, which are highly correlated with the blood vessel pattern on the cortical surface, because hemodynamic noise is most pronounced at blood vessels. For this correlation, it is crucial to record a high-contrast image of the blood vessel pattern, which can be imaged with green light. This is important since it avoids particularly that components containing mainly pixel noise are used for extraction. To this end, components are standardized and squared, causing both an increase and a decrease in blood vessel reflectance to yield a positive value. The resulting components are then ordered according to their correlation coefficient with the low pass filtered

(Gaussian filter, 100 mm<sup>2</sup>) image of the blood vessel pattern. The first twelve components are used for extraction, twelve being a somewhat arbitrary number, which proved, however, most suitable for the BVE. We also tested other methods to define the optimal number of these components, none of which improved the performance of the BVE (see below). In particular, selecting fluctuation components based on a fixed threshold of the correlation coefficient between the blood vessel pattern and the fluctuation images was less effective than using a fixed number of components.

It is noteworthy, that the orthogonalization due to principal component analysis renders the selection of components insensitive to the order of the initial sequence of blank frames.

This selection process does not exclude the possibility that the fluctuation images also contain patterns evoked by neuronal stimulation. Therefore, the spatial pattern of stimulus driven activation must be independent of the blood vessel pattern. This is not necessarily true, but needs to be tested for each system and species. For instance, in macaque monkey primary visual cortex the blood vessel density differs between blob and inter-blob regions (Purves and LaMantia, 1993). Similarly, blood vessels follow the shape of barrels in rat somatosensory cortex (Patel, 1983). For the test data from cat as well as rodent visual cortex, however, this prerequisite seems to be well satisfied (correlation coefficients between extensively averaged raw maps and blood vessel pattern for cat:  $0.020 \pm 0.014$ , mice:  $-0.022 \pm 0.007$  rat:  $-0.015 \pm 0.028$ , error: standard error of the mean, SEM).

Fluctuation components can be defined and selected in multiple ways. We tested the following options for the determination of fluctuations, none of which markedly improved the BVE:

We evaluated an independent component analysis (Bell and Sejnowski, 1995) instead of the principal component analysis. In addition, we examined various thresholds for the selection of the fluctuation components. Given the prerequisite that stimulus related and fluctuation images are not correlated, one could imagine to employ this lack of correlation to determine the thresholds for the fluctuation images. To this end, we selected fluctuation images, which exhibited the highest ratio of their correlation with the blood vessel pattern and the correlation with the raw stimulus images averaged over all available trials. This procedure did not improve blood vessel extraction, most likely because also the averaged stimulus image does contain blood vessel related artifacts. Thence, those noise components are excluded from the extraction, which are most prominent in the stimulus image.

### **III.1.2.2 Extraction**

After computing the hemodynamic fluctuations, a criterion is needed to determine adequate extraction. As one criterion, we propose the minimization of the correlation coefficient between the stimulus image and the fluctuations. Given that the stimulus image contains noise, which is uncorrelated to the stimulus induced activity pattern, the correlation between the stimulus image and the fluctuation components should be zero. A linear extraction satisfies this criterion with the extraction coefficients  $\mathbf{I}$  being equal to the correlation between stimulus image  $s$  and orthogonalized fluctuation components  $p_k$ .

$$(1) \quad \begin{aligned} s_{BVE} &= s - \sum_k \mathbf{I}_k p_k \\ \mathbf{I}_k &= \text{corr}(s, p_k) \end{aligned}$$

As a second criterion, we suggest the minimization of the standard deviation over space of the stimulus image. This criterion is motivated by the assumption that hemodynamic noise increases the spatial standard deviation. Again, if neuronal activation and fluctuations are uncorrelated, the contribution of the fluctuations to the spatial standard deviation across the stimulus image should be minimized.

Given a linear extraction  $s_{BVE} = s - \sum_k \mathbf{I}_k p_k$ ,  $\mathbf{I}_k = \text{corr}(s, p_k)$  minimizes standard deviation ( $\Delta s_{BVE}$ ) over all pixels  $s(\mathbf{x})$ .

Proof: Let  $s$  and  $p$  be standardized.

$$\begin{aligned} \frac{\partial \Delta s_{BVE}}{\partial \mathbf{I}} &= \frac{\partial}{\partial \mathbf{I}} \left( \sum_{\mathbf{x}} s(\mathbf{x})^2 - 2\mathbf{I} p(\mathbf{x})s(\mathbf{x}) + \mathbf{I}^2 p(\mathbf{x})^2 \right) \\ &= \sum_{\mathbf{x}} 2\mathbf{I} p(\mathbf{x})^2 - 2p(\mathbf{x})s(\mathbf{x}) \end{aligned}$$

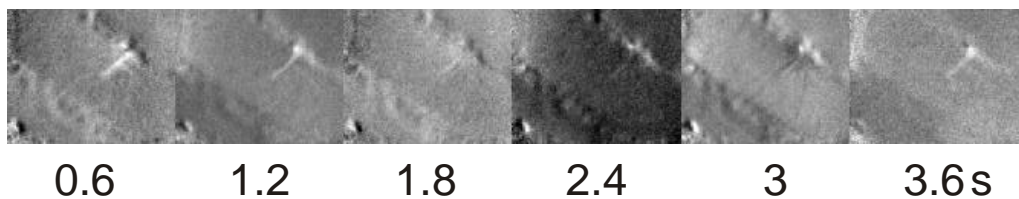
Thence, at  $\mathbf{I} = \text{corr}(s, p)$   $\frac{\partial \Delta s_{BVE}}{\partial \mathbf{I}}$  is zero and  $\Delta s_{BVE}$  reaches its only minimum. Given that multiple components  $p_k$  are orthogonal, we obtain (1).

Because of the linearity of (1) as well as the similarity of the means and variances of single stimulus frames, one can average the frame sequence before extraction. The errors introduced by this are small and are outweighed by the multi-fold increase in speed. The CPU time on a 500 Mhz, 512 MB RAM Pentium PC necessary for BVE is only 2-5 times longer than the conventional analysis, i.e., it is approx. 2-10 min, depending on the number of stimulus conditions and trials.

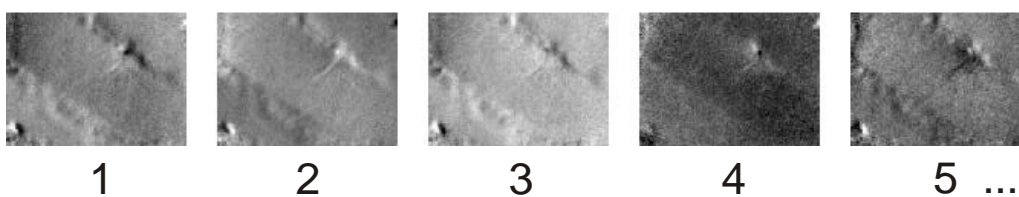
This algorithm was applied to trials, which was the average of six repetitions of the same stimulus. Applying the BVE to single repetition trials would further increase blood vessel

extraction. However, the residual correlation of the fluctuation images with the stimulus image can interfere with the recorded activation pattern. To determine the true neuronal activity pattern, trials consisting of an average of six repetitions proved most appropriate. In any case, the linearity of (1) renders the BVE relatively insensitive to the order of averaging and extraction.

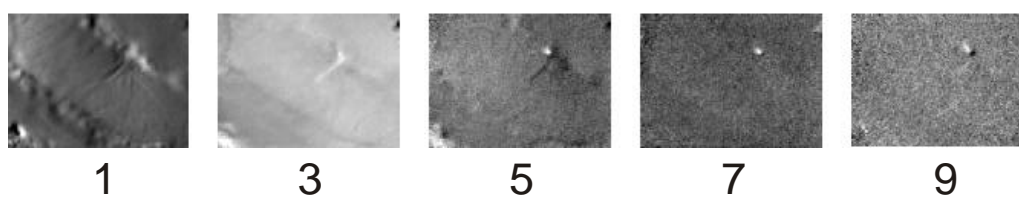
# 1. Blank Sequence



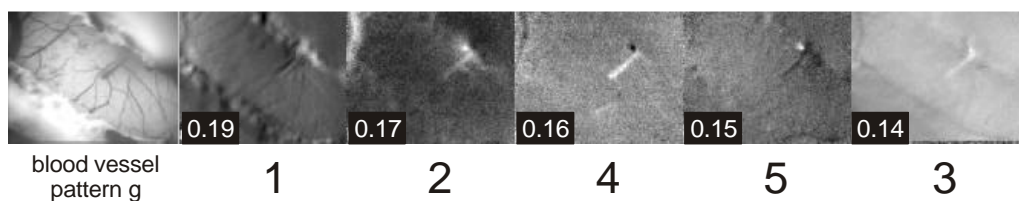
# 2. Fluctuations



# 3. PCA



# 4. Correlate with Blood Vessel Pattern

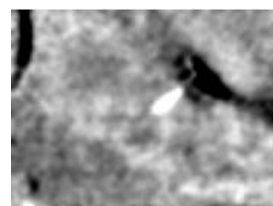
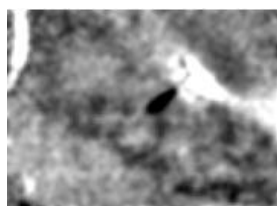


# 5. Linear Extraction

Raw Image

BVE

Difference



We explored a number of modifications of the algorithm used for the extraction, none of which noticeably improved the BVE:

Neither denoising using a sigma filter nor high or low pass filtering before computation of the correlation between stimulus images yielded a better performance. Similarly, the use of higher order components of the fluctuation images did not improve the performance of the algorithm. This observation substantiates the assumption implicit in (1) that the raw stimulus image is a linear combination of hemodynamic noise and neuronal activation.

## III.2 Results

Ongoing and stimulus related hemodynamic fluctuations can seriously impede high-resolution optical imaging (Bonhoeffer and Grinvald, 1996; Mayhew et al., 1996; Chen-Bee et al., 1996; Chen-Bee et al., 2000). This problem is particularly severe in rats, where large blood vessels are often present on the cortical surface. The BVE extracts most of these fluctuations, thus allowing reproducible, high-resolution optical imaging in rodents. Also, in cat visual cortex, the BVE

**Figure 24 (previous page): Illustration of the BVE algorithm applied to images from cat visual cortex. The cortex was stimulated with a horizontal grating activating approximately half of the visible cortical surface:**

**Interleaved with the recording of the blank corrected stimulus images  $s_i$  with  $i: 0, \dots, n-1$  frames per stimulus an additional image sequence is taken without visual stimulation, a so-called blank  $b_i$ ,  $i: 0 \dots n-1$  (for display purposes displayed here with correction with the averaged blank).**

**To reveal fluctuations  $f_j$  in the blank sequence subsequent frames are divided by each other:**

$$f_j = b_j - b_{j+1}, \quad j: 0, \dots, n-2.$$

**To decompose these images into a limited number of independent blood vessel artifacts a principal component analysis is performed on the fluctuation images.**

**Some of these principal components  $p_j$  reflect fluctuations caused by blood vessels. The subset  $p_k$  of those is selected based on their correlation (printed in the dark box at lower left of each image) with a low-pass filtered image  $g$  of the blood vessel pattern (image on the left):**

$$\text{corr}\left(\left(p_k - \text{mean}(p_k)\right)^2, g\right).$$

**These selected components are linearly extracted from the stimulus images  $s_i$ :**

$$s'_i = s_i - \sum_k I_{ik} p_k.$$

**The coefficients  $I_{ik}$  are chosen to minimize correlation between  $s_i$  and  $p_k$  and the standard deviation over space for  $s_i$ :**

$$I_{ik} = \text{corr}(s_i, p_k).$$

improves the quality of functional imaging considerably.

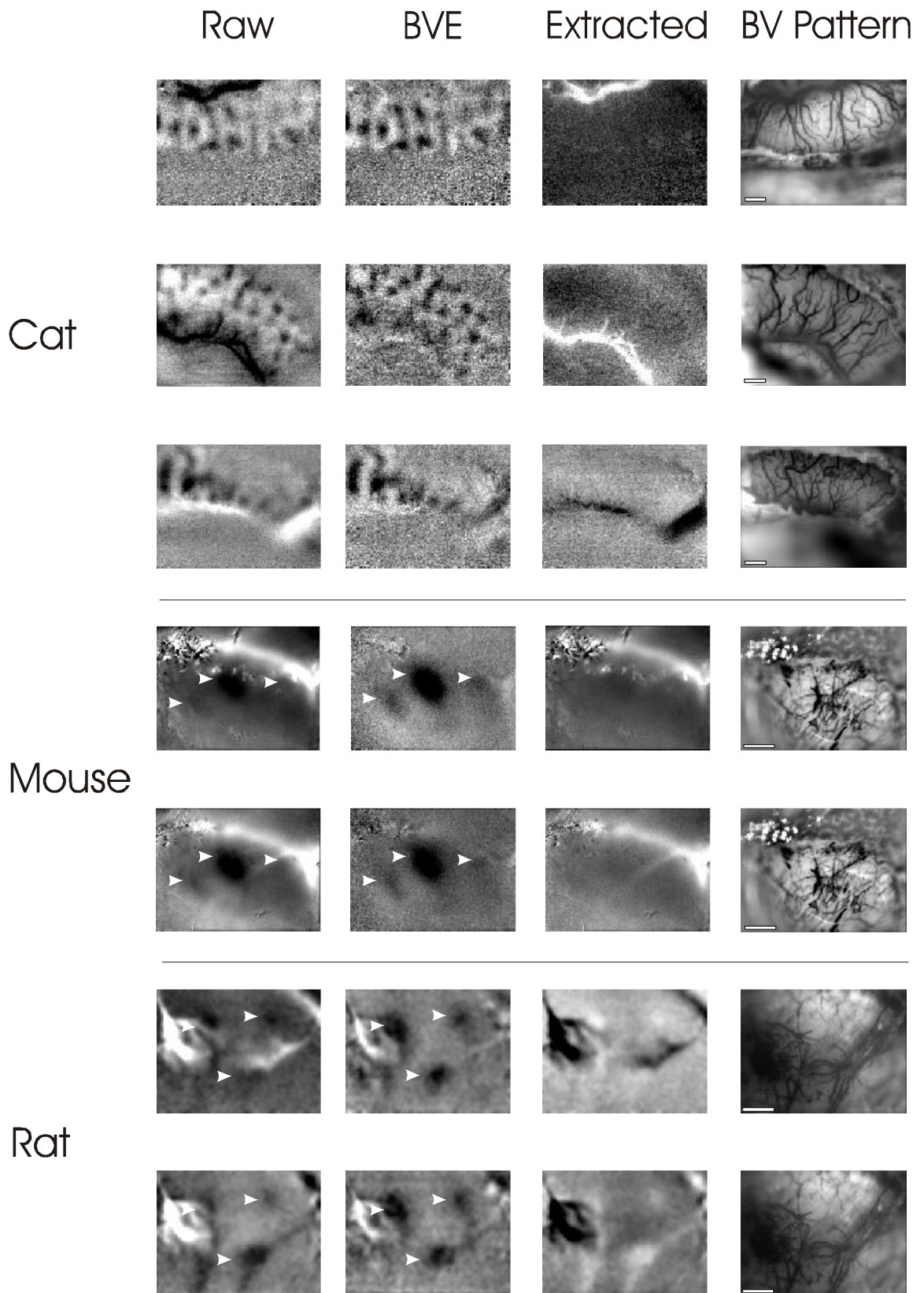
In Figure 25, we present examples of blood vessel extractions from optical imaging data obtained from cat, mice, and rat visual cortex. For cats, large draining veins within sulci often produce prominent blood vessel related artifacts in images of orientation domains. In most cases, these artifacts do not perturb the general impression of the imaged maps, but they can impede the quantification, particularly after high-pass filtering. Within the BVE images, these artifacts are virtually absent.

The images of mouse visual cortex are from the same animal and were acquired with the same retinotopic stimulus for both sets. Stimulation in this part of the visual field activates cortical regions in three different areas of the visual cortex (Schuett et al., 2001), but the prominent sinus overshadows the entire map in the raw images. The BVE extracts this huge blood vessel, and the three patches can be imaged with high reproducibility.

In rat visual cortex, image quality is lower than in cat and mice indicated by a lower inter-trial correlation (see below). In the example from rat visual cortex, a similar retinotopic stimulus was used, which also activated neurons in three different areas. Both sets of images were again obtained in subsequent trials in the same rat. As for mice, the BVE images in both sets are more similar to each other than the raw images. The similarity between the extracted image and the blood vessel pattern suggests that this increase in correlation is caused mainly by an extraction of blood vessel related artifacts.

To quantify the benefit of the BVE on image quality, we measured inter-trial correlation. For this purposes, we computed the correlation coefficient between subsequent trials in the cortical region where the stimuli elicited a neural response. We found that in all species (cats, rats, and mice, 3 animals tested for each species; 5-12 trials per animal; 6 repetitions per trial, 16-30 images from each trial), the BVE significantly increased inter-trial correlation ( $p < 0.01$ , t-test, Fig. 26a).

Particularly, while images from rats are of lower quality than images from cat and mice, the BVE increases the reproducibility of rat recordings slightly but significantly above the level of inter-trial correlation in unprocessed data from cat visual cortex, which might serve as a benchmark for the quality of optical imaging data ( $p = 0.0175$ , t-test). The increase in reproducibility, however, is restricted to regions, in which visual stimuli activate the cortex, but it does not occur at cortical regions outside the stimulated area, which we evaluated for control purposes. Hence, we conclude that the BVE does not increase inter-trial correlation *per se*, but only when an activity related signal is measured. Still, this increase in reproducibility does not exclude the possibility that the BVE introduces some sort of stimulus related artifact. Only the correlation with the true pattern of neuronal activation can be used to test this. As its best approximation for the genuine pattern of neuronal activation, we employed the mean across all trials (more than 4 trials).



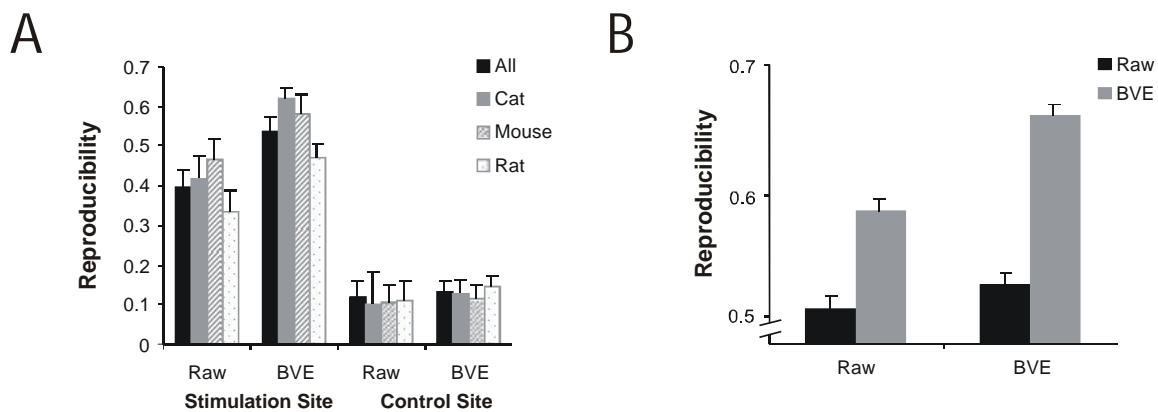


**Figure 26: The BVE increases inter-trial reproducibility. (A) Inter-trial correlation coefficients between different trials for cat, mouse, and rat at the stimulated cortical region and at the non-stimulated control region. Since the stimulated region was determined automatically by thresholding the maximum intensity projection of all single condition maps 2 SD above blank, a small residual positive correlation remains at the control region. Note that for all species the correlation coefficient is higher for the BVE trial than for the raw trials. (B) Correlation coefficients at the stimulation site between single trials and the corresponding averaged mean across 5 or more trials for both the raw and BVE mean and the raw and BVE trials, respectively. Again, the BVE increases the correlation coefficient for all tested animals compared to raw trials.**

To ensure that the BVE does not introduce artifacts, we computed the correlation coefficient between one trial and the raw mean of all trials except for the correlated one. We found a significantly higher correlation coefficient for the BVE trials with this raw mean in comparison to raw trials ( $p = 0.026$ , t-test, pooled across all animals, Fig. 26b). Again, this increase occurred only in the stimulated area and not at control sites. It is worth mentioning that the correlation of the single raw trials with the mean over the BVE trials is also significantly higher than the correlation between single raw trials and the raw mean (Fig. 26b). Expectedly, the most prominent difference occurred when we compared the raw single trial - raw mean correlation with the BVE single trial - BVE mean correlation, because blood vessel related artifacts are not completely averaged out in the mean of the raw maps.

These results substantiate that the BVE extracts only fluctuating noise and does not instill artifacts into optical imaging data in any of the tested species and systems. Therefore, the BVE seems to

**Figure 25 (previous page): Examples of BVE images from cat, mice, and rat: the first column displays the raw, blank corrected images, the second column the BVE images, the third column the extracted images (18-36 repetitions). Each set of images is scaled and clipped in the same way. The fourth column shows the corresponding blood vessel patterns. Scale bars: 1mm. The three cat images were obtained from different animals, all stimulated visually with whole field gratings of one orientation. The two sets of images from mouse and rat visual cortex were recorded in the same animal, respectively. An identical retinotopic stimulus was used in both cases, however, the images were acquired at different times to illustrate reproducibility. In the recordings of rodent visual cortex, activity in several visual areas is visible (arrowheads), in the BVE images. Note the improvement in quality in the BVE images in comparison to the raw images, as well as the similarity between the extracted images and the blood vessel patterns. Since the BVE removes mainly large structures, it resembles a selective high-pass filter. Thus, pixel noise appears more prominent in the BVE.**

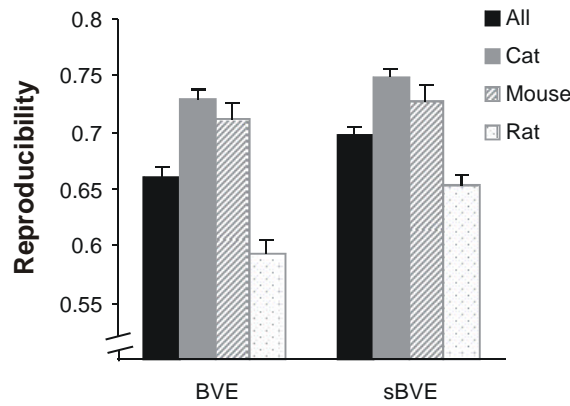


**Figure 27: Comparison of the correlation coefficients at the site of stimulation between the mean and single trials of the BVE and sBVE, respectively. The sBVE inter-trial correlation is higher in all cases. In particular, for low quality rat images, but also for cat and the average across all species the sBVE improves reproducibility significantly ( $p < 0.05$ , t-test) in comparison to the BVE.**

be a safe and reliable method to improve image quality and reproducibility of optical imaging data.

## Improvements of the BVE

We tested a number of modifications of the BVE to determine the options with the best performance. Most of these variants did not improve reproducibility; only one elaboration proved useful, particularly for low quality data with strong hemodynamic noise:

Although the fluctuations derived from blank sequences capture a major part of hemodynamic noise, hemodynamic fluctuations arising during stimulus presentation can exhibit different spatial patterns. To determine these fluctuations, we used, in addition to the blank sequence, an imaging sequence obtained during stimulus presentation. Both sequences were high-pass filtered and processed by the principal component analysis. The further selection process was the same as for the basic BVE described in the previous sections. This stimulus related BVE (sBVE) is based on the assumption that the high-resolution component of the intrinsic signal reaches a plateau level after approximately 2 s (Malonek and Grinvald, 1996) and subsequent fluctuations contain mainly hemodynamic changes due to blood volume changes.

The sBVE algorithm scores significantly better than the BVE on both the correlations with the raw mean and the correlation with the mean across the BVE and the sBVE images, respectively. This increase in reproducibility is most pronounced for low quality rat images.

However, care must be taken to ensure that only those stimulus frames are used for sBVE, in which the high-resolution optical signal has reached a plateau. Otherwise, the pattern of neuronal activation will be distorted. In all tested cases this prerequisite was met, as indicated by the low correlation coefficient between the extracted images and the raw mean also for the sBVE (BVE:

0.165±0.011, sBVE: 0.178±0.011). In any case, we recommend comparing the BVE images with those yielded by the sBVE and carefully evaluating the extracted images when using the sBVE.

### III.3 Discussion

A number of different analysis methods based on statistical analysis of the signal time course have been devised to improve optical imaging data, (Cannestra et al., 1996; Everson et al., 1997; Stetter et al., 2000; Gabbay et al., 2000). However, none of those studies used the blood vessel pattern to determine potential artifacts. While our method might be less universally applicable than these general-purpose signal analysis techniques, it might be more powerful for optical imaging, since it incorporates additional information on the likely position of potential artifacts. Unfortunately, in none of the above reports the potential improvement in image quality gained by the algorithm has been quantified by determining the inter-trial correlation of real optical imaging data. We believe that this criterion is crucial for the testing of any analysis method, as the method should be carefully evaluated when a new species or cortical region is imaged for the first time. Such quantifications can also provide a benchmark for comparisons in imaging quality. For instance, our studies proved that optical imaging in cat and mouse visual cortex are of similar quality, while rat recordings are less well reproducible.

To enhance such low quality data, we developed the BVE. We have shown that the BVE is capable of improving optical recordings in rat above the level of reproducibility in conventionally processed cat data. Averaging over all species, reproducibility can be increased by up to 20 %. Such an improvement might be crucial for optical imaging under circumstances, when large blood vessels cause prominent artifacts. Additionally, the BVE allows shortening the acquisition time necessary for high quality imaging, which in turn leaves time for complicated stimulus arrangements. Importantly, the BVE might be particularly useful for intra-operative imaging in humans (Haglund et al., 1992), where time is limited and blood vessel related artifacts can be very pronounced.

The BVE is a fast algorithm, which is only about three times slower than the fast standard processing of optical imaging data; hence, it can be routinely employed.

Interestingly, the BVE does not interfere with the time course of the intrinsic signal, since the order of the initial image stack is left intact. Therefore, this algorithm can be combined with all other signal improvement techniques based on the analysis of the time course of the intrinsic signal (Cannestra et al., 1996; Everson et al., 1997; Stetter et al., 2000; Gabbay et al., 2000). It will be interesting to explore potential additional improvements in inter-trial correlation due to combination of the BVE with these methods.

Blood vessel artifacts are also prominent in optical imaging with voltage sensitive dyes *in vivo* (Grinvald et al., 1994; Shoham et al., 1999) and they might conflict with high-resolution functional magnetic resonance imaging (Kim et al., 2000). We therefore expect it to be beneficial to adapt this approach improving reproducibility and image quality in these methods as well.

## Summary

The study reported in the first part of this thesis utilized optical imaging of intrinsic signals to visualize changes in orientation maps in cat visual cortex induced by pairing a visual stimulus with an intracortical electrical stimulation. We found that the direction of plasticity within orientation maps depends critically on the relative timing between visual and electrical stimulation on a millisecond time scale: a shift in orientation preference towards the paired orientation was observed if the cortex was first visually and then electrically stimulated. In contrast, the cortical response to the paired orientation was diminished if the electrical preceded the visual cortical stimulation. Spike-time-dependent plasticity has been observed in single cell studies; however, our results demonstrate an analogous effect at the systems level in the live animal. Thus, timing-dependent plasticity needs to be incorporated into our conception of cortical map development.

While the pairing paradigm induced pronounced shifts in orientation preference, the general setup of the orientation preference map remained unaltered. In order to unravel potential factors contributing to this overall stability, we determined the distribution of plasticity across the cortical surface. We found that pinwheel centers, points where domains of all orientation meet, exhibited less plasticity than other regions of the orientation map. The resistance of pinwheel centers to changes in orientation preference may support maintenance of the general structure of the orientation map.

The study that forms the second part employs optical imaging to visualize the retinotopy in mouse visual cortex. We were able to resolve the pattern of retinotopic activity with high precision and reliability in the primary visual cortex (area 17). Functional imaging of the position, size and shape of area 17 corresponded exactly to the location of this area in stained histological sections. The imaged maps were also confirmed with electrophysiological recordings. The retinotopic structure of area 17 showed very low inter-animal variability, thus allowing averaging maps across animals and therefore statistical analysis. These averaged maps greatly facilitated the identification of at least four extrastriate visual areas. In addition, we detected decreases in the intrinsic signal below baseline with a shape and location reminiscent of lateral inhibition. This decrease of the intrinsic signal was shown to be correlated with a decrease in neuronal firing rate below baseline.

Both studies were facilitated by the development of a signal analysis technique (part III), which improves the quality of optical imaging data. Intrinsic signal fluctuations originating from blood vessels were minimized based on their correlation with the actual superficial blood vessel pattern. These fluctuation components were then extracted from images obtained during sensory

stimulation. This method increases the reproducibility of functional maps from cat, rat, and mouse visual cortex significantly and might also be applied to high resolution imaging using voltage sensitive dyes or functional magnetic resonance.

## References

1. Ackermann,R.F., Finch,D.M., Babb,T.L., and Engel,J. (1984). Increased glucose metabolism during long-duration recurrent inhibition of hippocampal pyramidal cells. *Journal of Neuroscience* 4, 251-264.
2. Albus,K. (1975). A quantitative study of the projection area of the central and the paracentral visual field in area 17 of the cat. I. The precision of the topography. *Experimental Brain Research* 24, 159-179.
3. Antonini,A., Fagiolini,M., and Stryker,M.P. (1999). Anatomical correlates of functional plasticity in mouse visual cortex. *Journal of Neuroscience* 19, 4388-4406.
4. Antonini,A. and Stryker,M.P. (1993). Rapid remodeling of axonal arbors in the visual cortex. *Science* 260, 1819-1821.
5. Azzopardi,P. and Cowey,A. (1993). Preferential representation of the fovea in the primary visual cortex. *Nature* 361, 719-721.
6. Baier,H. and Bonhoeffer,F. (1992). Axon guidance by gradients of a target-derived component. *Science* 255, 472-475.
7. Bell,A.J. and Sejnowski,T.J. (1995). An information-maximization approach to blind separation and blind deconvolution. *Neural Computation* 7, 1129-1159.
8. Berman,N., Payne,B.R., Labar,D.R., and Murphy,E.H. (1982). Functional organization of neurons in cat striate cortex: variations in ocular dominance and receptive-field type with cortical laminae and location in visual field. *Journal of Neurophysiology* 48, 1362-1377.
9. Berson,M. and Stean,J.J. (1995). Retinotopic Organization of the superior colliculus in relation to the retinal distribution of afferent ganglion cells. *Visual Neuroscience* 12, 671-686.
10. Bi,G.Q. and Poo,M.M. (1998). Synaptic modifications in cultured hippocampal neurons: dependence on spike timing, synaptic strength, and postsynaptic cell type. *Journal of Neuroscience* 18, 10464-10472.
11. Blakemore,C. and Cooper,G.F. (1970). Development of the brain depends on the visual environment. *Nature* 228, 477-478.

12. Blasdel,G.G. (1992). Differential imaging of ocular dominance and orientation selectivity in monkey striate cortex. *Journal of Neuroscience* 12, 3115-3138.
13. Blasdel,G.G. and Salama,G. (1986). Voltage-sensitive dyes reveal a modular organization in monkey striate cortex. *Nature* 321, 579-585.
14. Bliss,T.V. and Gardner-Medwin,A.R. (1971). Long-lasting increases of synaptic influence in the unanesthetized hippocampus. *Journal of Physiology* 216, 32P-33P.
15. Bonhoeffer,T. and Grinvald,A. (1991). Iso-orientation domains in cat visual cortex are arranged in pinwheel-like patterns. *Nature* 353, 429-431.
16. Bonhoeffer,T. and Grinvald,A. (1996). Optical imaging based on intrinsic signals. The methodology. In *Brain Mapping: The Methods*, A. W. Toga and J. C. Mazziotta, eds. (London: Academic Press), pp. 55-97.
17. Borg-Graham,L.J., Monier,C., and Fregnac,Y. (1998). Visual input evokes transient and strong shunting inhibition in visual cortical neurons. *Nature* 393, 369-373.
18. Bosking,W.H., Zhang,Y., Schofield,B., and Fitzpatrick,D. (1997). Orientation selectivity and the arrangement of horizontal connections in tree shrew striate cortex. *Journal of Neuroscience*. 17, 2112-2127.
19. Cannestra,A.F., Blood,A.J., Black,K.L., and Toga,A.W. (1996). The evolution of optical signals in human and rodent cortex. *Neuroimage* 3, 202-208.
20. Caviness,V.S. (1975). Architectonic map of neocortex of the normal mouse. *Journal of Comparative Neurology* 164 , 247-263.
21. Chapman,B. and Gödecke,I. (2000). Cortical cell orientation selectivity fails to develop in the absence of ON-center retinal ganglion cell activity. *Journal of Neuroscience* 20, 1922-1930.
22. Chapman,B. and Stryker,M.P. (1993). Development of orientation selectivity in ferret visual cortex and effects of deprivation. *Journal of Neuroscience* 5251-5622.
23. Chen-Bee,C.H., Kwon,M.C., Masino,S.A., and Frostig,R.D. (1996). Areal extent quantification of functional representations using intrinsic signal optical imaging. *Journal of Neuroscience Methods* 68, 27-37.
24. Chen-Bee,C.H., Polley,D.B., Brett-Green,B., Prakash,N., Kwon,M.C., and Frostig,R.D. (2000). Visualizing and quantifying evoked cortical activity assessed with intrinsic signal imaging. *J Neurosci.Methods* 97, 157-173.

25. Cheng,H.J. and Flanagan,J.G. (1994). Identification and cloning of ELF-1, a developmentally expressed ligand for the Mek4 and Sek receptor tyrosine kinases. *Cell* 79, 157-168.
26. Chung,S. and Ferster,D. (1998). Strength and orientation tuning of the thalamic input to simple cells revealed by electrically evoked cortical suppression. *Neuron* 20, 1177-1189.
27. Collins,R.C. (1978). Use of cortical circuits during focal penicillin seizures: an autoradiographic study with [14C]deoxyglucose. *Brain Research* 150, 487-501.
28. Coogan,T.A. and Burkhalter,A. (1993). Hierarchical organization of areas in rat visual cortex. *Journal of Neuroscience* 13, 3749-3772.
29. Crair,M.C., Gillespie,D.C., and Stryker,M.P. (1998). The role of visual experience in the development of columns in cat visual cortex. *Science* 279, 566-570.
30. Crair,M.C., Ruthazer,E.S., Gillespie,D.C., and Stryker,M.P. (1997). Relationship between the ocular dominance and orientation maps in visual cortex of monocularly deprived cats. *Neuron* 19, 307-318.
31. Crowley,J.C. and Katz,L.C. (1999). Development of ocular dominance columns in the absence of retinal input [see comments]. *Nature Neuroscience* 2, 1125-1130.
32. Crowley,J.C. and Katz,L.C. (2000). Early development of ocular dominance columns. *Science* 290, 1321-1324.
33. Cusick,C.G. and Lund,R.D. (1981). The distribution of the callosal projection to the occipital visual cortex in rats and mice. *Brain Research*. 214, 239-259.
34. Daniel,P.M. and Whitteridge,D. (1961). The representation of the visual field on the cerebral cortex in mokey. *Journal of Physiology* 159, 203-221.
35. Daw,N.W., Fox,K., Sato,H., and Czepita,D. (1992). Critical period for monocular deprivation in the cat visual cortex. *Journal of Neurophysiology* 67, 197-202.
36. Debanne,D., Gähwiler,B.H., and Thompson,S.M. (1994). Asynchronous pre- and postsynaptic activity induces associative long- term depression in area CA1 of the rat hippocampus in vitro. *Proceedings of the National Academy of Sciences of the United States of America* 91, 1148-1152.
37. Debanne,D., Gähwiler,B.H., and Thompson,S.M. (1998). Long-term synaptic plasticity between pairs of individual CA3 pyramidal cells in rat hippocampal slice cultures. *Journal of Physiology* 507, 237-247.
38. Dräger,U.C. and Olsen,J.F. (1981). Ganglion cell distribution in the retina of the mouse. *Investigative Ophthalmology & Visual Science* 20, 285-293.

39. Dräger,U.C. (1975). Receptive fields of single cells and topography in mouse visual cortex. *Journal of Comparative Neurology* 160, 269-290.
40. Drescher,U., Kremoser,C., Handwerker,C., Loschinger,J., Noda,M., and Bonhoeffer,F. (1995). In vitro guidance of retinal ganglion cell axons by RAGS, a 25 kDa tectal protein related to ligands for Eph receptor tyrosine kinases. *Cell* 82, 359-370.
41. Duffy,K.R., Murphy,K.M., and Jones,D.G. (1998). Analysis of the postnatal growth of visual cortex. *Visual Neuroscience* 831-899.
42. Espinoza,S.G. and Thomas,H.C. (1983). Retinotopic organization of striate and extrastriate visual cortex in the hooded rat. *Brain Research* 137-144.
43. Everson,R., Knight,B.W., and Sirovich,L. (1997). Separating spatially distributed response to stimulation from background. I. Optical imaging. *Biological Cybernetics* 77, 407-417.
44. Eysel,U.T., Shevelev,I.A., Lazareva,N.A., and Sharaev,G.A. (1998). Orientation tuning and receptive field structure in cat striate neurons during local blockade of intracortical inhibition. *Neuroscience* 84, 25-36.
45. Feldman,D.E. (2000). Timing-based LTP and LTD at vertical inputs to layer II/III pyramidal cells in rat barrel cortex. *Neuron* 27, 45-56.
46. Ferrer,J.M., Price,D.J., and Blakemore,C. (1988). The organization of corticocortical projections from area 17 to area 18 of the cat's visual cortex. *Proceedings of the Royal Society of London - Series B: Biological Sciences* 233, 77-98.
47. Ferster,D., Chung,S., and Wheat,H. (1996). Orientation selectivity of thalamic input to simple cells of cat visual cortex. *Nature* 380, 249-252.
48. Freeman,R.D. and Pettigrew,J.D. (1973). Alteration of visual cortex from environmental asymmetries. *Nature* 246 , 359-360.
49. Fregnac,Y., Shulz,D., Thorpe,S., and Bienenstock,E. (1988). A cellular analogue of visual cortical plasticity. *Nature* 333, 367-370.
50. Fregnac,Y., Shulz,D., Thorpe,S., and Bienenstock,E. (1992). Cellular analogs of visual cortical epigenesis. I. Plasticity of orientation selectivity. *Journal of Neuroscience* 12, 1280-1300.
51. Fregnac,Y. and Shulz,D.E. (1999). Activity-dependent regulation of receptive field properties of cat area 17 by supervised Hebbian learning. *Journal of Neurobiology* 41, 69-82.

52. Frisen,J., Yates,P.A., McLaughlin,T., Friedman,G.C., O'Leary,D.D., and Barbacid,M. (1998). Ephrin-A5 (AL-1/RAGS) is essential for proper retinal axon guidance and topographic mapping in the mammalian visual system. *Neuron* 20, 235-243.
53. Frostig,R.D., Lieke,E.E., Ts'O,D.Y., and Grinvald,A. (1990). Cortical functional architecture and local coupling between neuronal activity and the microcirculation revealed by in vivo high-resolution optical imaging of intrinsic signals. *Proceedings of the National Academy of Sciences of the United States of America* 87, 6082-6086.
54. Gabbay,M., Brennan,C., Kaplan,E., and Sirovich,L. (2000). A principal components-based method for the detection of neuronal activity maps: application to optical imaging. *Neuroimage* 11, 313-325.
55. Girman,S.V., Sauve,Y., and Lund,R.D. (1999). Receptive field properties of single neurons in rat primary visual cortex. *Journal of Neurophysiology* 82, 301-311.
56. Gödecke,I., Kim,D.S., Bonhoeffer,T., and Singer,W. (1997). Development of orientation preference maps in area 18 of kitten visual cortex. *European Journal of Neuroscience* 9, 1754-1762.
57. Gödecke,I. and Bonhoeffer,T. (1996). Development of identical orientation maps for two eyes without common visual experience. *Nature* 379, 251-254.
58. Grinvald,A., Lieke,E., Frostig,R.D., Gilbert,C.D., and Wiesel,T.N. (1986). Functional architecture of cortex revealed by optical imaging of intrinsic signals. *Nature* 324, 361-364.
59. Grinvald,A., Lieke,E.E., Frostig,R.D., and Hildesheim,R. (1994). Cortical point-spread function and long-range lateral interactions revealed by real-time optical imaging of macaque monkey primary visual cortex. *Journal of Neuroscience* 14, 2545-2568.
60. Gustafsson,B., Wigström,H., Abraham,W.C., and Huang,Y.Y. (1987). Long term potentiation in the hippocampus using depolarizing current pulses as the conditioning stimulus to single volley synaptic potentials. *Journal of Neuroscience* 7(3), 774-780.
61. Haglund,M.M., Ojemann,G.A., and Hochman,D.W. (1992). Optical imaging of epileptiform and functional activity in human cerebral cortex. *Nature* 358, 668-671.
62. Hallett,P.E. (1987). The scale of the visual pathways of mouse and rat. *Biological Cybernetics* 57, 275-286.
63. Hebb,D.O. (1949). *The organization of behavior. A neuropsychological theory.* (New York: Wiley).
64. Hetherington,P.A. and Swindale,N.V. (1999). Receptive field and orientation scatter studied by tetrode recordings in cat area 17. *Visual Neuroscience* 16, 637-652.

65. Hirsch,H.V. and Spinelli,D.N. (1970). Visual experience modifies distribution of horizontally and vertically oriented receptive fields in cats. *Science* 168, 869-871.
66. Hubel,D. and Wiesel,T.N. (1963). Shape and arrangement of columns in cat's striate cortex. *Journal of Physiology (London)* 165, 559-568.
67. Hübener,M., Shoham,D., Grinvald,A., and Bonhoeffer,T. (1997). Spatial relationships among three columnar systems in cat area 17. *Journal of Neuroscience* 17, 9270-9284.
68. Ikeda,H. and Wright,M.J. (1975). The latency of visual cortical neurones in area 17 in the cat to visual stimuli with reference to the sustained (X) and transient (Y) and 'simple' and 'complex' cell classification. *Journal of Physiology* 245, 114-115.
69. Itasaki,N. and Nakamura,H. (1996). A role for gradient en expression in positional specification on the optic tectum. *Neuron* 16, 55-62.
70. Kim,D.S., Duong,T.Q., and Kim,S.G. (2000). High-resolution mapping of iso-orientation columns by fMRI. *Nature Neuroscience* 3, 164-169.
71. Kirkwood,A., Lee,H.K., and Bear,M.F. (1995). Co-regulation of long-term potentiation and experience-dependent synaptic plasticity in visual cortex by age and experience. *Nature* 375, 328-331.
72. Kirkwood,A., Silva,A., and Bear,M.F. (1997). Age-dependent decrease of synaptic plasticity in the neocortex of alphaCaMKII mutant mice. *Proceedings of the National Academy of Sciences of the United States of America* 94, 3380-3383.
73. Kojic,L., Dyck,R.H., Gu,Q., Douglas,R.M., Matsubara,J., and Cynader,M.S. (2000). Columnar distribution of serotonin-dependent plasticity within kitten striate cortex. *Proceedings of the National Academy of Sciences of the United States of America* 97, 1841-1844.
74. Komatsu,Y. and Iwakiri,M. (1993). Long-term modification of inhibitory synaptic transmission in developing visual cortex. *NeuroReport* 4, 907-910.
75. Kossut,M. and Singer,W. (1991). The effect of short periods of monocular deprivation on excitatory transmission in the striate cortex of kittens: a current source density analysis. *Experimental Brain Research* 85, 519-527.
76. Kossut,M., Thompson,I.D., and Blakemore,C. (1983). Ocular dominance columns in cat striate cortex and effects of monocular deprivation: a 2-deoxyglucose study. *Acta Neurobiologiae Experimentalis* 43, 273-282.

77. Lewis,J.W. and Olavarria,J.F. (1995). Two rules for callosal connectivity in striate cortex of the rat. *Journal of Comparative.Neurology* 361, 119-37.
78. MacVicar,B.A. and Hochman,D. (1991). Imaging of synaptically evoked intrinsic optical signals in hippocampal slices. *Journal of Neuroscience* 11, 1458-1469.
79. Maffei,L. and Bisti,S. (1976). Binocular interaction in strabismic kittens deprived of Vision. *Science* 191, 579-580.
80. Malach,R. (1989). Patterns of connections in rat visual cortex. *Journal of Neuroscience* 9, 3741-3752.
81. Maldonado,P.E., Gödecke,I., Gray,C.M., and Bonhoeffer,T. (1997). Orientation selectivity in pinwheel centers in cat striate cortex. *Science* 276, 1551-1555.
82. Malonek,D., Dirnagl,U., Lindauer,U., Yamada,K., Kanno,I., and Grinvald,A. (1997). Vascular imprints of neuronal activity: relationships between the dynamics of cortical blood flow, oxygenation, and volume changes following sensory stimulation. *Proceedings of the National Academy of Sciences of the United States of America* 94, 14826-14831.
83. Malonek,D. and Grinvald,A. (1996). Interactions between electrical activity and cortical microcirculation revealed by imaging spectroscopy: implications for functional brain mapping. *Science* 272, 551-554.
84. Malonek,D. and Grinvald,A. (1997). Vascular regulation at sub millimeter range. Sources of intrinsic signals for high resolution optical imaging. [Review] [18 refs]. *Advances in Experimental Medicine & Biology* 413, 215-220.
85. Mangini,N.J. and Pearlman,A.L. (1980). Laminar distribution of receptive field properties in the primary visual cortex of the mouse. *Journal of Comparative Neurology* 193, 203-222.
86. Mark,R., James,A.C., and Shen,X.M. (1993). Geometry of the representation of the visual field on the superior colliculus in the wallaby: 1. Normal Projection. *Journal of Comparative Neurology* 330, 303-314.
87. Markram,H., Lübke,J., Frotscher,M., and Sakmann,B. (1997). Regulation of synaptic efficacy by coincidence of postsynaptic APs and EPSPs. *Science* 275, 213-215.
88. Masino,S.A., Kwon,M.C., Dory,Y., and Frostig,R.D. (1993). Characterization of functional organization within rat barrel cortex using intrinsic signal optical imaging through a thinned skull. *Proceedings of the National Academy of Sciences of the United States of America* 90, 9998-10002.

89. Mayhew,J.E., Askew,S., Zheng,Y., Porrill,J., Westby,G.W., Redgrave,P., Rector,D.M., and Harper,R.M. (1996). Cerebral vasomotion: a 0.1-Hz oscillation in reflected light imaging of neural activity. *Neuroimage*. *4*, 183-193.
90. McLean,H.A., Caillard,O., BenAri,Y., and Gaiarsa,J.L. (1996). Bidirectional plasticity expressed by GABAergic synapses in the neonatal rat hippocampus. *Journal of Physiology-London* *496*, 471-477.
91. Metin,C., Godement,P., and Imbert,M. (1988). The primary visual cortex in the mouse: receptive field properties and functional organization. *Experimental Brain Research* *69*, 594-612.
92. Miller,K.D., Erwin,E., and Kayser,A. (1999). Is the development of orientation selectivity instructed by activity? *Journal of Neurobiology* *41*, 44-57.
93. Montero,V.M. (1993). Retinotopy of cortical connections between the striate cortex and extrastriate visual areas in the rat. *Experimental Brain Research* *94*, 1-15.
94. Movshon,J.A., Thompson,I.D., and Tolhurst,D.J. (1978). Spatial and temporal contrast sensitivity of neurones in areas 17 and 18 of the cat's visual cortex. *Journal of Physiology* *283*, 101-120.
95. Murphy,P.C. and Sillito,A.M. (1986). Continuity of orientation columns between superficial and deep laminae of the cat primary visual cortex. *Journal of Physiology* *381*, 95-110.
96. Mustari,M. and Cynader,M. (1981). Prior strabismus protects kitten cortical neurons from the effects of monocular deprivation. *Brain Research* *211*, 165-170.
97. Olavarria,J., Mignano,L.R., and Van Sluyters,R.C. (1982). Pattern of extrastriate visual areas connecting reciprocally with striate cortex in the mouse. *Experimental Neurology* *78*, 775-779.
98. Patel,U. (1983). Non-random distribution of blood vessels in the posterior region of the rat somatosensory cortex. *Brain Research* *289*, 65-70.
99. Prakash,N., Vanderhaeghen,P., Cohen-Cory,S., Frisén,J., Flanagan,J.G., and Frostig,R.D. (2000). Malformation of the functional organization of somatosensory cortex in adult ephrin-A5 knock-out mice revealed by *in vivo* functional imaging. *Journal of Neuroscience* *20*, 5841-5847.
100. Purves,D. and LaMantia,A. (1993). Development of blobs in the visual cortex of macaques. *Journal of Comparative Neurology*. *334*, 169-175.
101. Quevedo,C., Hoffmann,K.P., Husemann,R., and Distler,C. (1996). Overrepresentation of the central visual field in the superior colliculus of the pigmented and albino ferret. *Visual Neuroscience* *13*, 627-638.

102. Rattay,F. (1998). The basic mechanism for the electrical stimulation of the nervous system. *Neuroscience* 89, 335-346.
103. Reid,R.C. and Alonso,J.M. (1995). Specificity of monosynaptic connections from thalamus to visual cortex. *Nature* 378, 281-284.
104. Rosa,M.G. and Schmid,L.M. (1995). Magnification factors, receptive field images and point-image size in the superior colliculus of flying foxes: comparison with the primary visual cortex. *Experimental Brain Research* 102, 551-556.
105. Rubin,B.D. and Katz,L.C. (1999). Optical imaging of odorant representations in the mammalian olfactory bulb. *Neuron* 23, 499-511.
106. Rumberger,A., Tyler,C.J., and Lund,J.S. (2001). Intra- and inter-areal connections between the primary visual cortex V1 and the area immediately surrounding V1 in the rat. *Neuroscience* 102, 35-52.
107. Ruthazer,E.S. and Stryker,M.P. (1996). The role of activity in the development of long-range horizontal connections in area 17 of the ferret. *Journal of Neuroscience* 7253-7699.
108. Schuett,S., Bonhoeffer,T., and Hübener,M. (2000). Mapping of retinotopy in rat visual cortex by combined linear extraction and principle component analysis of optical imaging data. *European Journal of Neuroscience Abstracts*.
109. Sengpiel,F., Stawinski,P., and Bonhoeffer,T. (1999). Influence of experience on orientation maps in cat visual cortex. *Nature Neuroscience* 2, 727-732.
110. Sermasi,E., Tropea,D., and Domenici,L. (1999). Long term depression is expressed during postnatal development in rat visual cortex: a role for visual experience. *Developmental Brain Research* 113, 61-65.
111. Sharp,J.W., Gonzalez,M.F., Morton,M.T., Simon,R.P., and Sharp,F.R. (1988). Decreases of cortical and thalamic glucose metabolism produced by parietal cortex stimulation in the rat. *Brain Research* 438, 357-362.
112. Shatz,C.J. and Stryker,M.P. (1978). Ocular dominance in layer IV of the cat's visual cortex and the effects of monocular deprivation. *Journal of Physiology* 281, 267-283.
113. Shevelev,I.A., Eysel,U.T., Lazareva,N.A., and Sharaev,G.A. (1998). The contribution of intracortical inhibition to dynamics of orientation tuning in cat striate cortex neurons. *Neuroscience* 84, 11-23.

114. Shoham,D., Glaser,D.E., Arieli,A., Kenet,T., Wijnbergen,C., Toledo,Y., Hildesheim,R., and Grinvald,A. (1999). Imaging cortical dynamics at high spatial and temporal resolution with novel blue voltage-sensitive dyes. *Neuron* 24, 791-802.
115. Shouval,H.Z., Goldberg,D.H., Jones,J.P., Beckerman,M., and Cooper,L.N. (2000). Structured long-range connections can provide a scaffold for orientation maps. *Journal of Neuroscience* 20, 1119-1128.
116. Shulz,D.E., Sosnik,R., Ego,V., Haidarliu,S., and Ahissar,E. (2000). A neuronal analogue of state-dependent learning. *Nature* 403, 549-553.
117. Sillito,A.M. (1975). The effectiveness of bicuculline as an antagonist of GABA and visually evoked inhibition in the cat's striate cortex. *Journal of Physiology* 250, 287-304.
118. Simmons,P.A., Lemmon,V., and Pearlman,A.L. (1982). Afferent and efferent connections of the striate and extrastriate visual cortex of the normal and reeler mouse. *Journal of Comparative Neurology* 211, 295-308.
119. Simmons,P.A. and Pearlman,A.L. (1982). Retinotopic organization of the striate cortex (area 17) in the reeler mutant mouse. *Brain Research*. 256, 124-126.
120. Simmons,P.A. and Pearlman,A.L. (1983). Receptive-field properties of transcallosal visual cortical neurons in the normal and reeler mouse. *Journal of Neurophysiology* 50, 838-848.
121. Song,S., Miller,K.D., and Abbott,L.F. (2000). Competitive Hebbian learning through spike-timing-dependent synaptic plasticity. *Nature Neuroscience* 3, 919-926.
122. Stetter,M., Schiessl,I., Otto,T., Sengpiel,F., Hubener,M., Bonhoeffer,T., and Obermayer,K. (2000). Principal component analysis and blind separation of sources for optical imaging of intrinsic signals. *Neuroimage*. 11, 482-490.
123. Talbot,S.A. and Marshal,W.H. (1941). Physiological studies on neural mechanisms of visual localization and discrimination. *American Journal of Ophtamology* 24, 1255-1264.
124. Thomas,H.C. and Espinoza,S.G. - Relationships between interhemispheric cortical connections and visual areas in hooded rats. - *Brain Research*.1987.Aug.11; 417.(2):214.-24. 214-244.
125. Tootell,R.B., Switkes,E., Silverman,M.S., and Hamilton,S.L. (1988). Functional anatomy of macaque striate cortex. II. Retinotopic organization. *Journal of Neuroscience* 8, 1531-1568.
126. Trachtenberg,J.T., Trepel,C., and Stryker,M.P. (2000). Rapid extragranular plasticity in the absence of thalamocortical plasticity in the developing primary visual cortex. *Science* 287, 2029-2032.

127. Trepel,C., Duffy,K.R., Pegado,V.D., and Murphy,K.M. (1998). Patchy distribution of NMDAR1 subunit immunoreactivity in developing visual cortex. *Journal of Neuroscience* 18, 3404-3415.
128. Ts'O,D.Y., Frostig,R.D., Lieke,E.E., and Grinvald,A. (1990). Functional organization of primate visual cortex revealed by high resolution optical imaging. *Science* 249, 417-420.
129. Tusa,R.J., Palmer,L.A., and Rosenquist,A.C. (1978). The retinotopic organization of area 17 (striate cortex) in the cat. *Journal of Comparative Neurology* 177, 213-235.
130. Van Essen,D.C. (1979). Visual areas of the mammalian cerebral cortex. *Annual Review of Neuroscience* 2, 227-263.
131. Vanderhaeghen,P., Lu,Q., Prakash,N., Frisen,J., Walsh,C.A., Frostig,R.D., and Flanagan,J.G. (2000). A mapping label required for normal scale of body representation in the cortex. *Nature Neuroscience* 3, 358-365.
132. Vanzetta,I. and Grinvald,A. (1999). Increased cortical oxidative metabolism due to sensory stimulation: implications for functional brain imaging. *Science* 286, 1555-1558.
133. Wagor,E., Mangini,N.J., and Pearlman,A.L. (1980). Retinotopic organization of striate and extrastriate visual cortex in the mouse. *Journal of Comparative Neurology* 193, 187-202.
134. Waldvogel,D., van Gelderen,P., Muellbacher,W., Ziemann,U., Immisch,I., and Hallett,M. (2000). The relative metabolic demand of inhibition and excitation. *Nature* 406, 995-998.
135. Wässle,H., Grunert,U., Rohrenbeck,J., and Boycott,B.B. (1989). Cortical magnification factor and the ganglion cell density of the primate retina. *Nature* 341, 643-646.
136. Webster,W.R., Serviere,J., Martin,R., and Brown,M. (1985). Uncrossed and crossed inhibition in the inferior colliculus of the cat: a combined 2-deoxyglucose and electrophysiological study. *Journal of Neuroscience* 5, 1820-1832.
137. Weliky,M. and Katz,L.C. (1997). Disruption of orientation tuning in visual cortex by artificially correlated neuronal activity. *Nature* 386, 680-685.
138. Wiesel,T.N. and Hubel,D. (1963a). Single cell responses in striate cortex of kittens deprived of vision in one eye. *Journal of Neurophysiology* 26, 1003-1017.
139. Wiesel,T.N. and Hubel,D. (1963b). Effects of visual deprivation on morphology and physiology of cells in the cat's lateral geniculate body. *Journal of Neurophysiology* 26, 978-993.
140. Wong-Riley,M. (1979). Changes in the visual system of monocularly sutured or enucleated cats demonstrable with cytochrome oxidase histochemistry. *Brain Research* 171, 11-28.

141. Zhang,L.I., Tao,H.W., Holt,C.E., Harris,W.A., and Poo,M. (1998). A critical window for cooperation and competition among developing retinotectal synapses. *Nature* 395, 37-44.

# *Curriculum Vitae*

## *Personal Data*

<b>Name, Surname</b>	Schuett, Sven
<b>Date of Birth</b>	08/18/1972

## *Education*

<b>School</b>	08/78 – 06/91	Abitur at Hohe Landesschule Hanau
<b>Civil Service</b>	07/91 – 09/92	child care and geriatrics
<b>University</b>	10/92 – 01/95	Undergraduate studies in physics and philosophy at the University of Göttingen, intermediate exam in philosophy, Vordiplom in physics
	02/95 – 12/95	Received Diploma for Graduates in neuroscience and Award in Science from the University of Otago, New Zealand
	04/96 – 10/99	Postgraduate studies in physics and philosophy at the University of Bremen
	11/98	Diplom in physics "Goal learning with dynamic reinforcement functions"
	10/99	Magister in philosophy "Evaluation of models in physics and neuroscience"
	03/99 – now	Work on Ph.D. thesis at the Max-Planck-Institute of Neurobiology, Munich.

